J. Fluid Mech. (2004), *vol.* 508, *pp.* 287–317. © 2004 Cambridge University Press
DOI: 10.1017/S0022112004009188 Printed in the United Kingdom

The nonlinear evolution of a wavetrain emanating from a point source in a boundary layer

By MARCELLO A. F. MEDEIROS†

Departamento de Engenharia Mecânica, Pontifícia Universidade Católica de Minas Gerais, Av. Dom José Gaspar, 500, Belo Horizonte, 30535-610 – MG, Brazil

(Received 16 July 2003 and in revised form 26 January 2004)

The paper reports on an investigation into the nonlinear evolution of a wavetrain emanating from a point source in a flat-plate boundary layer. The work was mainly experimental, but calculations using linear and nonlinear stability theory and parabolized stability equations were also performed to support the conclusions. The amplitudes of the disturbances used were very small and, as a consequence, turbulence was not reached within the experimental domain. Nevertheless, interesting nonlinear behaviour was observed. The nonlinear regime was characterized by the appearance of a three-dimensional mean flow distortion in the form of longitudinal streaks. It was possible to distinguish two different stages of the nonlinear regime. In the first stage, the streak pattern displayed relatively low spanwise wavenumbers. The pattern appeared to have grown algebraically from a pair of counter-rotating streamwise vortices. Weakly nonlinear calculations suggested that the vortices arise from the interaction of the spanwise and the wall-normal velocity components. The second stage exhibited more streaks and higher spanwise wavenumbers. This stage was found to be associated with a peak-and-valley structure of the wave amplitude. A remarkable feature was that the streamwise position of the onset of the second stage of the nonlinear regime was not affected by the amplitude of the disturbance. Parabolized stability calculations suggested that the peak-and-valley structure was the outcome of a secondary instability of the fundamental type. An interaction similar to that of the first nonlinear stage involving the waves composing the peak-and-valley structure yielded other streamwise vortices and hence a different streak pattern. The results also suggested that, because the wave amplitudes were very small, the linear stability influenced the nonlinear evolution. Indeed, the onset of the second stage of the nonlinear regime appeared to be associated with the proximity of the second branch of the linear stability diagram.

1. Introduction

Work on natural transition can be traced back to the pioneering experiments of Schubauer & Skramstad (1943). However, prediction of the onset of turbulence in natural transition is still a challenge. Transition in boundary layers often involves the amplification of Tollmien–Schlichting waves. When these waves become large, different nonlinear mechanisms can take place. In the H-type transition, also called N-type, a secondary instability appears and the growth of subharmonic waves is observed

† Present address: Departamento de Engenharia de Materiais, Aeronáutica e Automobilística, Escola de Engenharia de São Carlos – Universidade de São Paulo, Brazil; marcello@sc.usp.br.

https://doi.org/10.1017/S0022112004009188 Published online by Cambridge University Press

(Herbert 1988; Kachanov 1994). On the other hand, in the K-type transition the secondary instability is of the fundamental type (Klebanoff, Tidstrom & Sargent 1962; Herbert 1988; Kachanov 1994). There is also the oblique transition, which is concerned with the evolution of a pair of oblique waves (Schmid & Henningson 1992; Berlin, Lundbladh & Henningson 1994; Elofsson & Alfredsson 1998; Reddy *et al.* 1998). In this case, transition is preceded by the formation of streamwise vortices and the appearance of three-dimensional mean flow distortions in the form of longitudinal streaks.

In natural transition, features that are characteristic of these transition scenarios have been reported. For instance, the formation of longitudinal streaks was observed in the experiments carried out by Westin *et al.* (1994) and Boiko *et al.* (1994). In other experiments (Shaikh 1997) the process appeared to be dominated by the growth of subharmonic waves. Experiments have also shown that, just before turbulence sets in, spikes are observed in natural transition. Spikes are often recognized as a key ingredient of the K-type transition (Klebanoff *et al.* 1962).

This state of affairs is not to be considered surprising. In the H-type, K-type and oblique-type transition, the experimental conditions are tuned to produce a particular outcome. Indeed, in these experiments, the flow is perturbed with only a limited number of waves. In uncontrolled conditions, the perturbation is composed of a large number of modes and certainly all of these nonlinear interactions are possible.

In the current paper, the nonlinear evolution of a wavetrain emanating from a point source is studied. This is intended as a wave system that is more generic than those that lead directly to the transition routes described above, but still far less complicated than natural transition. This simpler model might provide an important step towards the understanding of natural transition. There the waves are three-dimensional and modulated, here only three-dimensionality is included.

This type of wavetrain has been studied elsewhere (Mack 1985; Kachanov *et al.* 1985; Seifert 1990; Seifert & Wygnanski 1991; Wiegand *et al.* 1995). However, these studies were restricted to the linear regime. A numerical simulation of the nonlinear regime of such a wavetrain has also been reported (Stemmer, Kloker & Wagner 1998). There, the nonlinear regime was found to involve the generation of streamwise vortices and the associated longitudinal streaks. The outcome was attributed to a mechanism of oblique transition.

The results shown here confirm that longitudinal streaks play an important role in the nonlinear evolution of the wavetrain emanating from a point source. It was also found that the process could be split into two stages. In the first stage, the generation of streaks was driven by a weakly nonlinear interaction that was in many ways similar to that observed in oblique transition. However, because it involved a large number of waves, it could display some different features.

The second stage was found to be governed by secondary instability of the fundamental type. The results also suggested that the second branch of the stability loop played an important role in generating the seeds for the resonating three-dimensional modes. The study is mainly based on wind-tunnel experiments, but theoretical explanations using linear stability calculations, weakly nonlinear analysis and simulations via the parabolized stability equations are also given to support the conclusions.

2. Brief description of the experimental procedures

The experiments to be reported here were carried out in a low-turbulence wind-tunnel at the Cambridge University Engineering Department.† The boundary layer

† This tunnel is now located at the Queen Mary & Westfield College of the University of London.

https://doi.org/10.1017/S0022112004009188 Published online by Cambridge University Press

developed on a 1.68 m long aluminium flat plate. The free-stream velocity was 17.3 m s^{-1}. The free-stream turbulence level was 0.008%, in the spectral range of 1 Hz to 5 kHz. A small loudspeaker was buried in the plate and connected to the flow through a 0.3 mm diameter hole at 203 mm from the leading edge of the plate. The loudspeaker that produced the perturbations was controlled by a computer. The streamwise velocity was measured with a constant temperature hot-wire anemometer. Further details of the experimental facility and the mean flow characteristics can be found in Medeiros & Gaster (1999*a*).

The study was aimed at investigating the implications of three-dimensionality to natural transition. Therefore, it was decided that the magnitude of the perturbations should be similar to those that cause turbulence in natural transition. It has been shown that the highly modulated and three-dimensional waves that occur naturally lead to transition at very low amplitudes (Gaster 1978; Shaikh 1997; Medeiros & Gaster 1999*a*, *b*). The excitation amplitudes used here were based on experiments with wavepackets carried out by Medeiros & Gaster (1999*a*). The small amplitudes used meant that turbulence was not reached within the experimental domain.

Figure 1 shows the evolution of the wavetrain along the centreline of the plate at $0.6\delta^*$ from the wall, where δ^* is the displacement thickness. In the figure, a scale indicates the amplitude of the oscillations. The wavetrain used was not actually continuous, but it was so long that its central part behaved like a continuous one. The idea was to treat the wavetrain as an event and use phase-averaging techniques to improve the signal to noise ratio. The data acquisition system was phase-locked to the excitation. The velocity records shown in the paper are the result of the ensemble average of 64 events. As shown in § 3, the standard deviation of the single realizations from the ensemble-averaged records was bellow 2% of the peak-to-peak amplitude of the perturbation velocity.

In the nonlinear regime, the signal displays a mean flow distortion. Because the disturbance velocity was so small, the 12-bit buffer did not have enough resolution to capture both the base and the disturbance velocity. Using an analogue filter to remove the direct current was considered inadequate because it would almost certainly affect the measurement of the mean flow distortion. In order to reduce the direct current level, a device was used to subtract a constant voltage from the total signal. This was later added to the voltage samples prior to their transformation into velocity records.

Care was taken that the ramps at the ends of the wavetrain were so gentle that streamwise-modulation effects became unimportant. It was also verified that the length of the wavetrain did not affect the results. Figure 2 shows the evolution of a wavetrain with longer end ramps and a shorter amplitude-constant central part. It is seen that the evolution was not sensitive to these effects.

3. Experimental observations

From figure 1, it appears that the nonlinear regime begins at about 700 mm from the leading edge of the plate. Initially, the mean flow distortion is negative, but further downstream it becomes positive. For comparison, figure 3 gives the evolution of the wave in the linear stability diagram for two-dimensional waves. At $x = 900$ mm, the waves have already crossed the second branch of the stability loop. Indeed in that region, along the centreline, the oscillations decay (figure 1). It is possible that the attenuation is linked to the linear stability. In spite of that, the nonlinear activity is still significant, as indicated by the large mean flow distortions attained at 1000 mm and 1100 mm from the leading edge.

https://doi.org/10.1017/S0022112004009188 Published online by Cambridge University Press

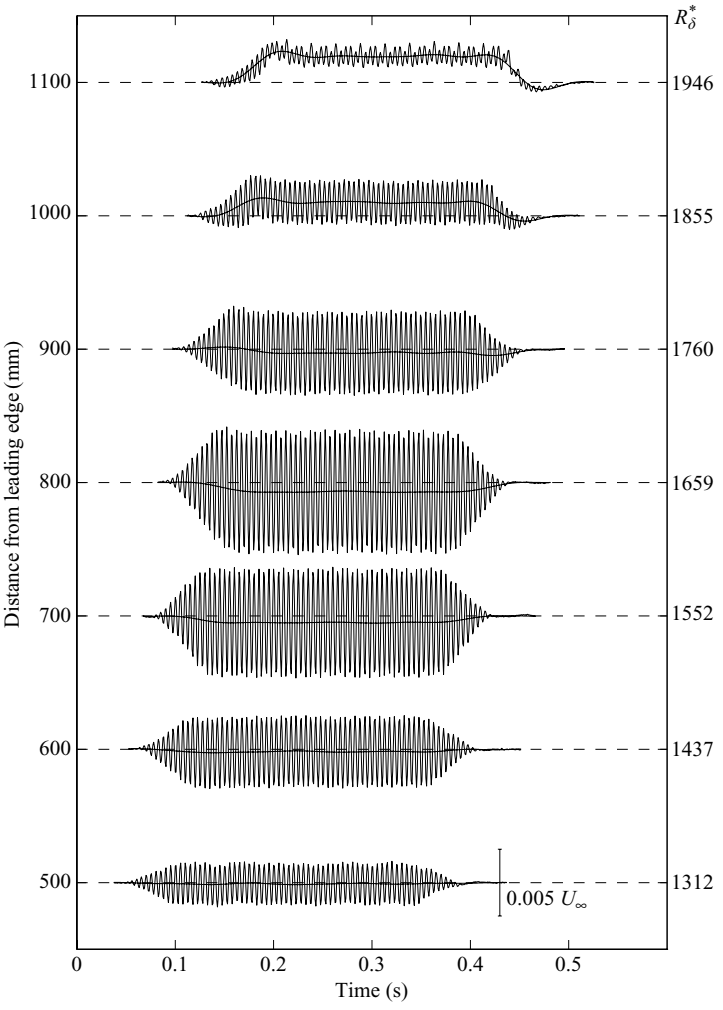


FIGURE 1. Streamwise evolution of the wavetrain along the centreline of the plate at $0.6\delta^*$ from the wall. The amplitude of the wave is given by the scale shown with the record at $x = 500$ mm.

Figure 4 displays the wavetrain evolution along the centreline in Fourier space. It represents the spectra of the ensemble-averaged signals. The oscillating part corresponds to a frequency of 200 Hz. The picture also shows that no significant signs of either subharmonic or harmonic oscillations are seen throughout the wave evolution. Definitely, the nonlinear behaviour is dominated by the mean flow distortion, represented by the very low-frequency signal.

Streamwise velocity records were also taken off the centreline of the plate. The results are shown for different streamwise distances in figure 5. The horizontal coordinate is the time. The frames cover periods of 0.156 s starting at different instants t_0. The vertical coordinate of each frame is the spanwise direction and covers up to 30 cm centred on the centreline of the plate. In the linear regime, the lines of constant phase form crescents. As the wave progresses, they span a larger portion of the flow field. In the nonlinear regime, the crescents look increasingly distorted. Despite many attempts, the reason for the asymmetrical behaviour close to the disturbance source

https://doi.org/10.1017/S0022112004009188 Published online by Cambridge University Press

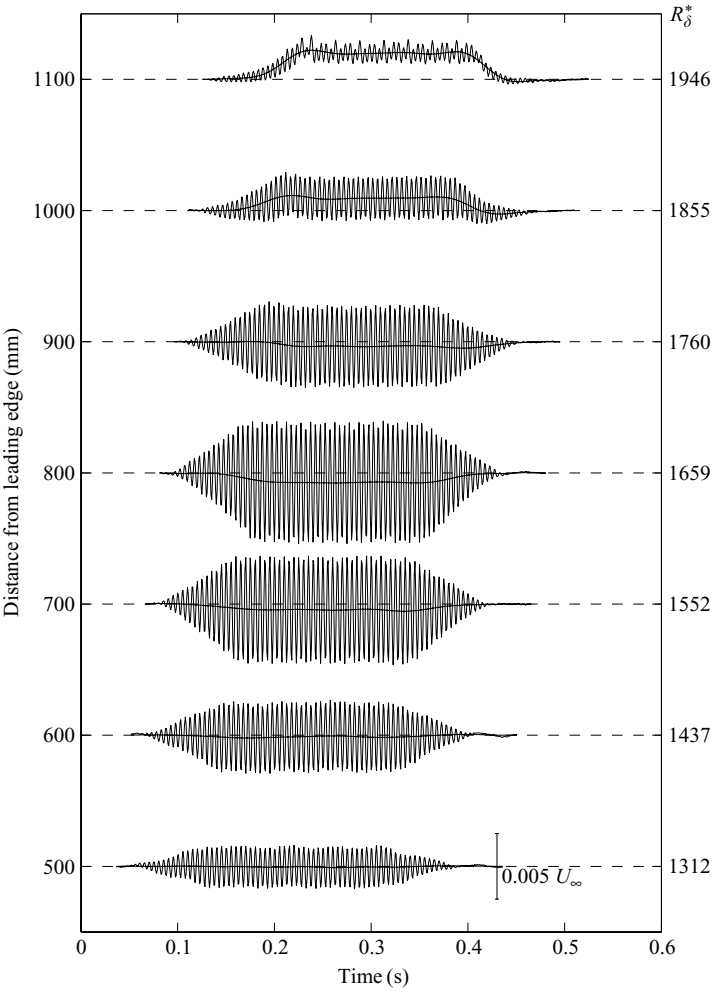


FIGURE 2. Streamwise evolution of a wavetrain with gentler ramps and a shorter central part as compared to that of figure 1.

could not be found. However, since this is much less marked further downstream, it was considered that this would not significantly affect the results in the nonlinear regime.

Despite the apparently strong nonlinear activity, turbulence was not reached within the experimental domain. In fact, the standard deviation of the original single realizations from the ensemble-averaged records remained very small throughout the evolution (figure 6). Note that here the axes are changed with respect to those of figure 5. The top left-hand corners of the frames of figure 5 correspond to the bottom right-hand corners in figure 7. However, the frames cover identical time × span domains. This facilitates the comparison between the different streamwise stations. The boundary-layer response to the excitation was very repeatable.

A clearer view of the nonlinear mean flow distortion is obtained if the oscillating part of the signal is digitally filtered out. Based on figure 4, it was considered that the mean flow distortion was contained within the components equal to and below 15 Hz. This was the cutoff frequency selected for the filter. In figures 1 and 2, the filtered

https://doi.org/10.1017/S0022112004009188 Published online by Cambridge University Press

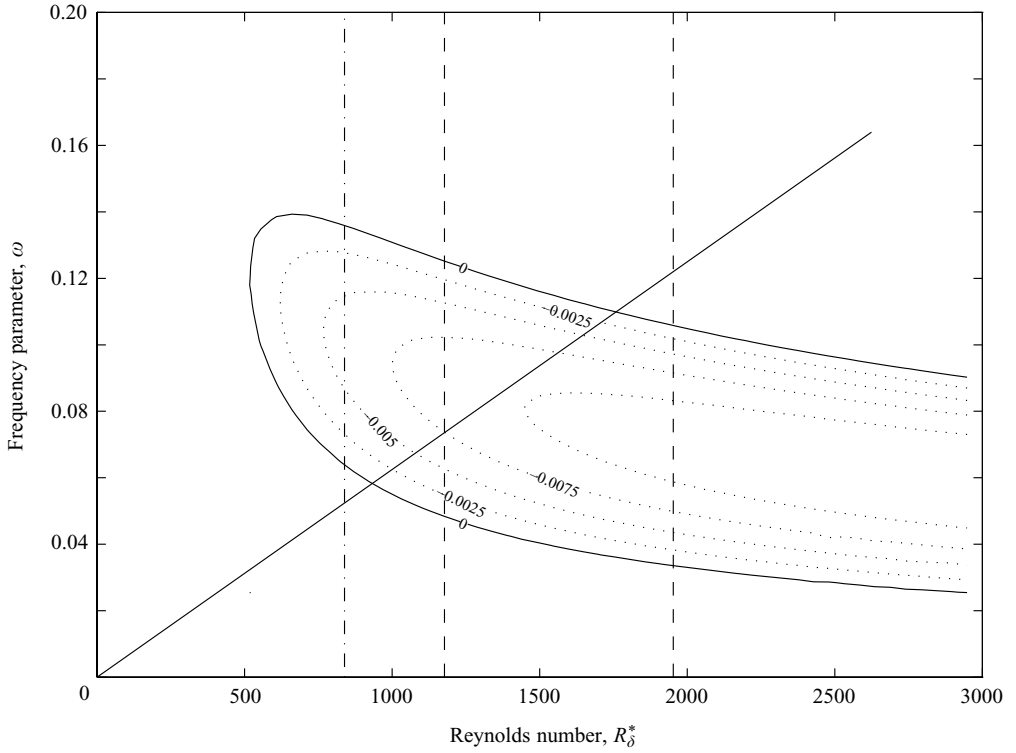


FIGURE 3. Evolution of the dominant two-dimensional wave in the stability loop, shown by the solid straight line. The dashed lines indicate the first and the last streamwise measuring stations. The dashed-dotted line marks the excitation source.

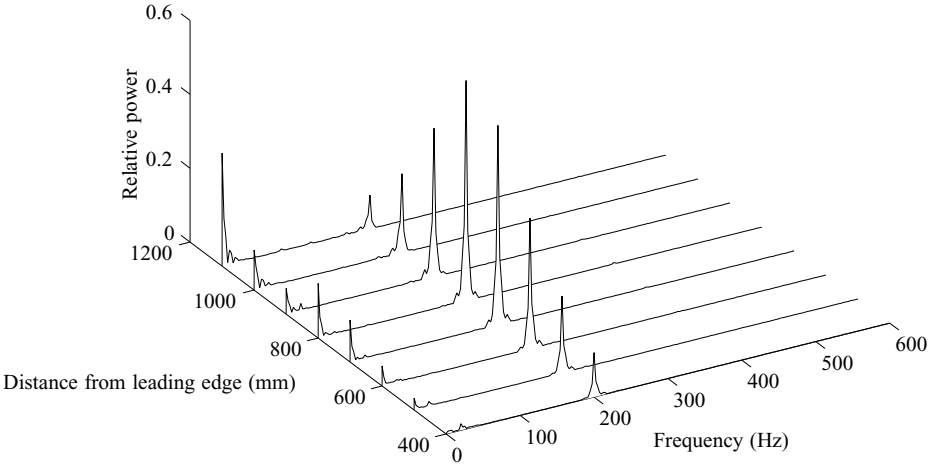


FIGURE 4. Streamwise evolution of the wavetrain at $0.6\delta^*$ from the wall along the centreline in Fourier space.

signals are also given and clearly indicate the mean flow distortions of the velocity field. Figure 7 presents the spanwise distribution of the mean flow distortion. Again, the frames are changed with respect to those of figure 5.

https://doi.org/10.1017/S0022112004009188 Published online by Cambridge University Press

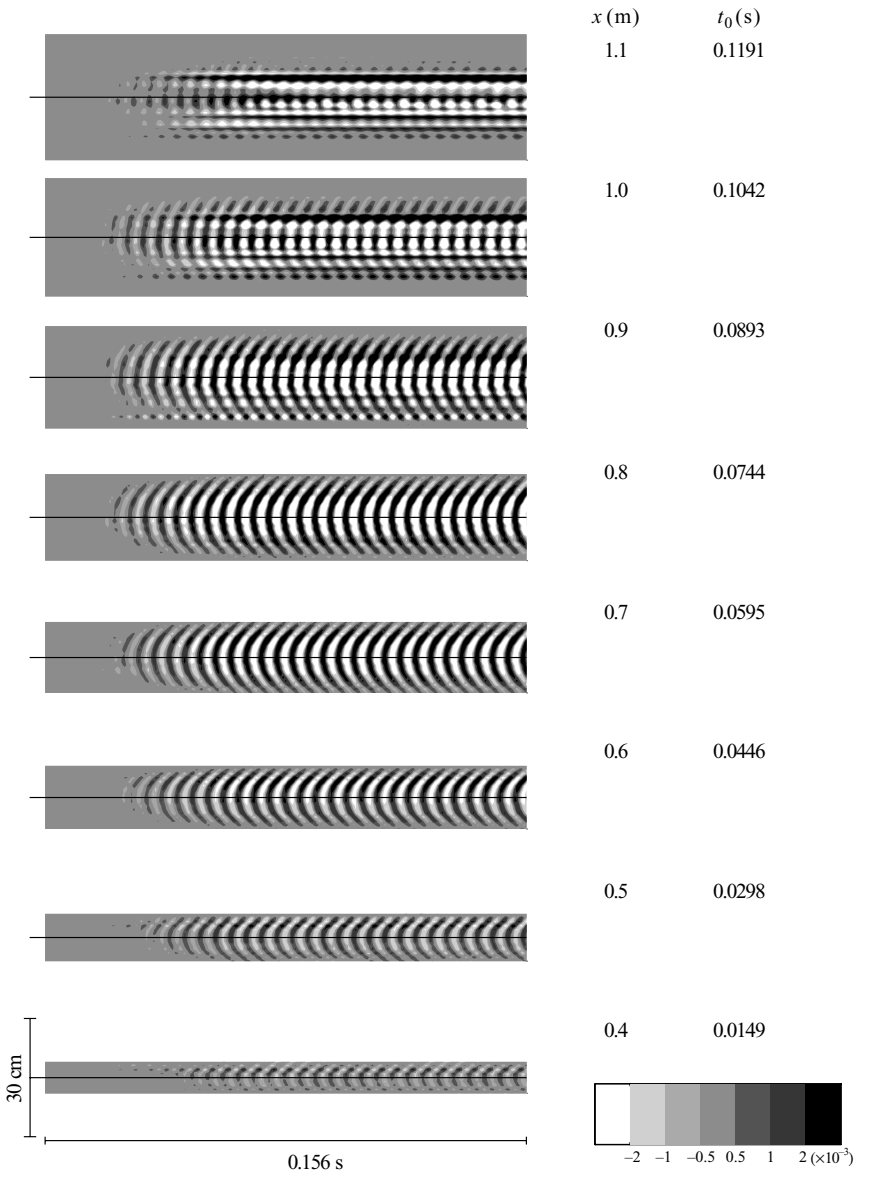


FIGURE 5. Streamwise evolution of the wavetrain at $0.6\delta^*$ from the wall shown by span × time planes. Note that each frame starts at a different t_0. The grey scale gives the velocity magnitude relative to the free-stream velocity. At each measuring station, the spanwise domain was restricted to the extent of the wavetrain.

Initially, no mean flow distortion is observed, since the wave system behaves linearly. At $x = 800$ mm, it can be seen that the mean flow distortion is, in fact, three-dimensional. The picture is not very symmetrical, but shows a negative central streak and one positive at each side of the centreline.

Longitudinal streaks are observed in many transitional or turbulent flows and are almost always related to the existence of longitudinal vorticity. It is known that, in a boundary layer, the velocity field associated with this vorticity promotes a redistribution of longitudinal momentum (Henningson, Lundbladh & Johansson

https://doi.org/10.1017/S0022112004009188 Published online by Cambridge University Press

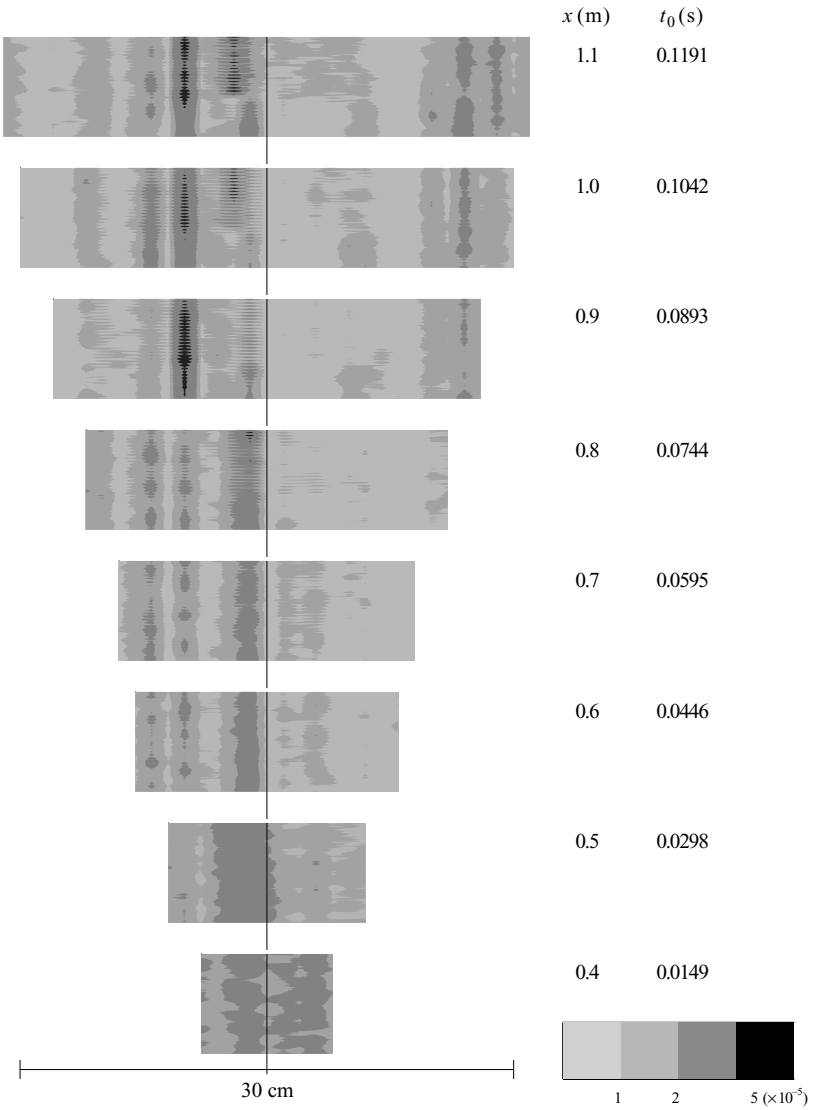


FIGURE 6. The standard deviation of the original single realizations from the ensemble-averaged time histories at $y = 0.6\delta^*$. Note that the frames are changed with respect to figure 5. The grey scale gives the magnitude relative to the free-stream velocity.

1993). At some places, low-momentum fluid is lifted away from the wall whereas at other places high-momentum fluid is moved closer to the wall. This is often referred to as the lift-up mechanism. The phenomenon promotes the transient or algebraic growth of the longitudinal streaks (Berlin *et al.* 1994; Elofsson & Alfredsson 1998) and produces the characteristic pattern. This is a key feature of the route to turbulence called oblique transition (Reddy *et al.* 1998). The numerical simulations reported by Stemmer *et al.* (1998) have also shown that in the wavetrain emanating from a point source, the appearance of the streaks was a result of streamwise vorticity. In the current investigation, the streamwise vorticity was not measured. However, from $x = 700$ mm to $x = 900$ mm the results were consistent with these ideas. The streaks

https://doi.org/10.1017/S0022112004009188 Published online by Cambridge University Press

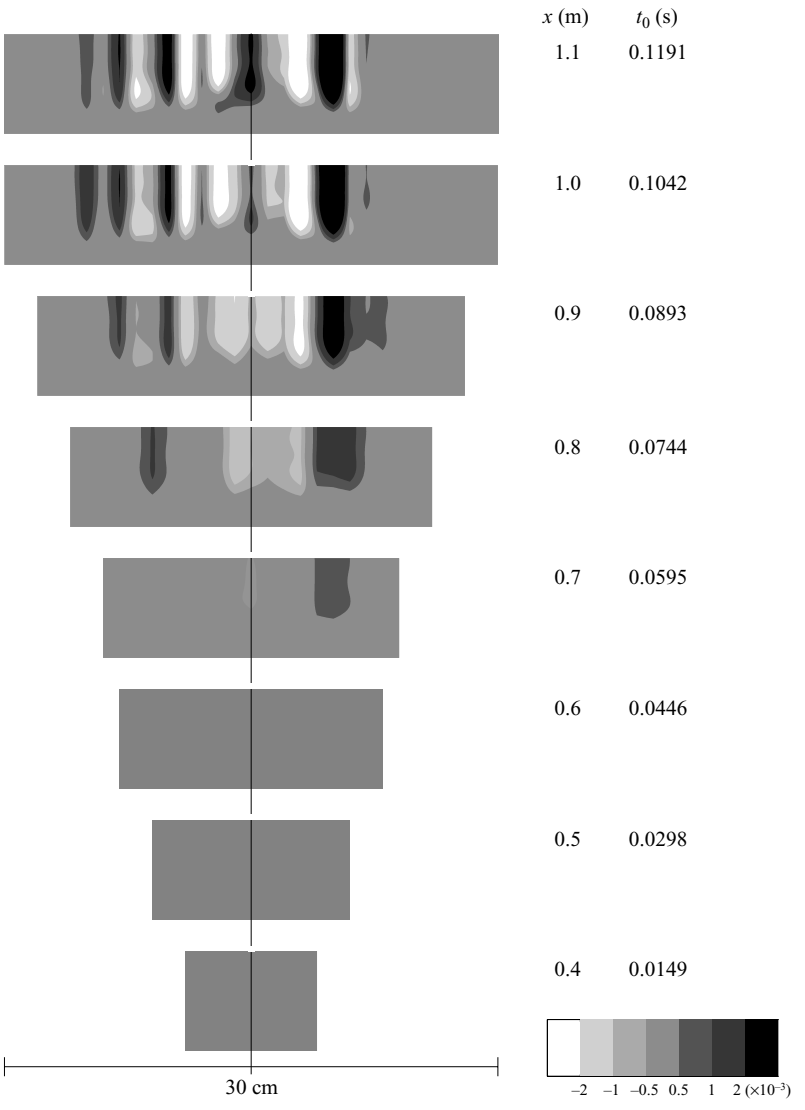


FIGURE 7. Streamwise evolution of the three-dimensional mean flow distortion at $0.6\delta^*$ from the wall shown by span × time planes. The grey scale gives the velocity magnitude relative to the free-stream velocity.

were therefore considered evidence of the existence of two regions of longitudinal vorticity of opposite sign.

At $x = 1000$ mm, a positive streak arises at the centre and splits the negative streak into two. This corresponds to the change of sign observed on the centreline evolution (figure 1). The newly created streak becomes wider at $x = 1100$ mm. Although the picture is not symmetric, the results tend to suggest that other streaks appear, particularly at the edges of the wave-system.

The evolution of the streaks in Fourier space is shown in figure 8. At station $x = 700$ mm, the first indication of the streaks is a mode of low spanwise wavenumber, centred at about $\beta = \pm 0.07$. Further downstream, $x = 1000$ mm and 1100 mm, the spectra is dominated by higher spanwise wavenumbers.

https://doi.org/10.1017/S0022112004009188 Published online by Cambridge University Press

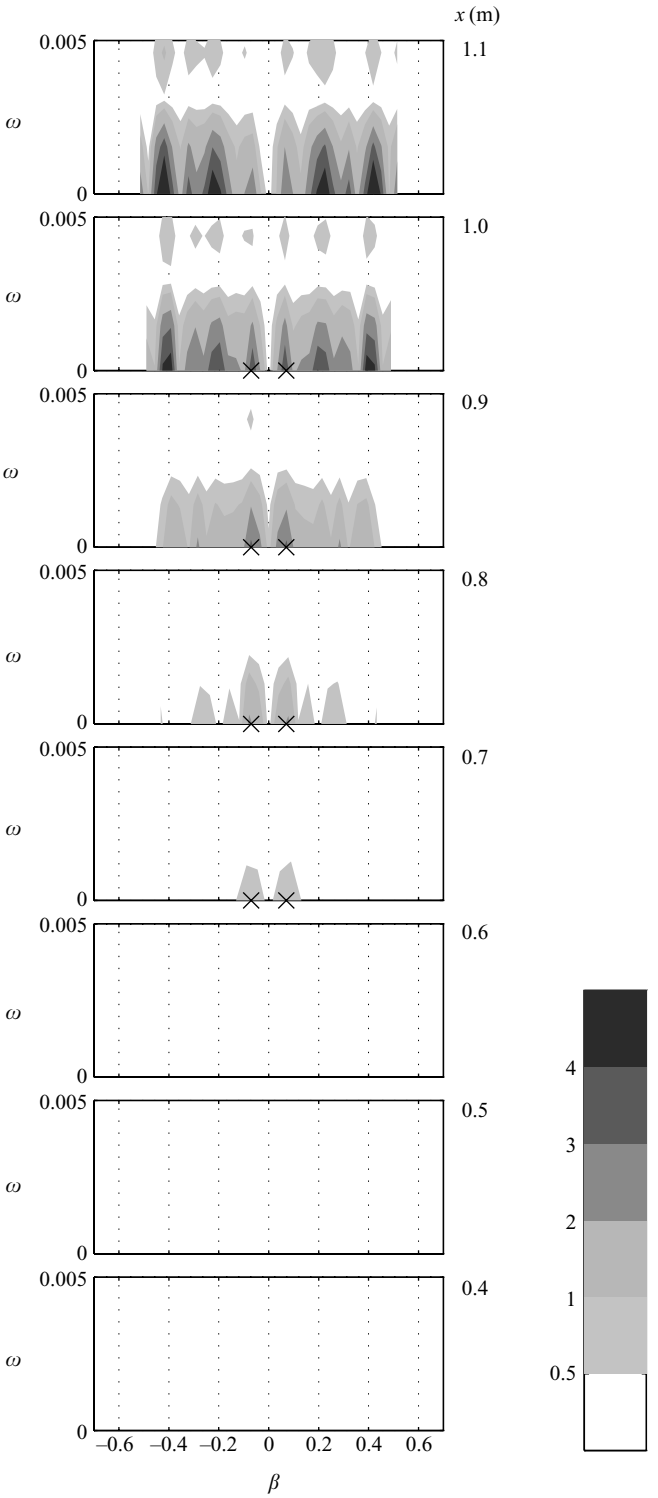


FIGURE 8. Streamwise evolution of the three-dimensional mean flow distortion in Fourier space. The grey scale indicates the relative power. The symbols indicate theoretical predictions.

https://doi.org/10.1017/S0022112004009188 Published online by Cambridge University Press

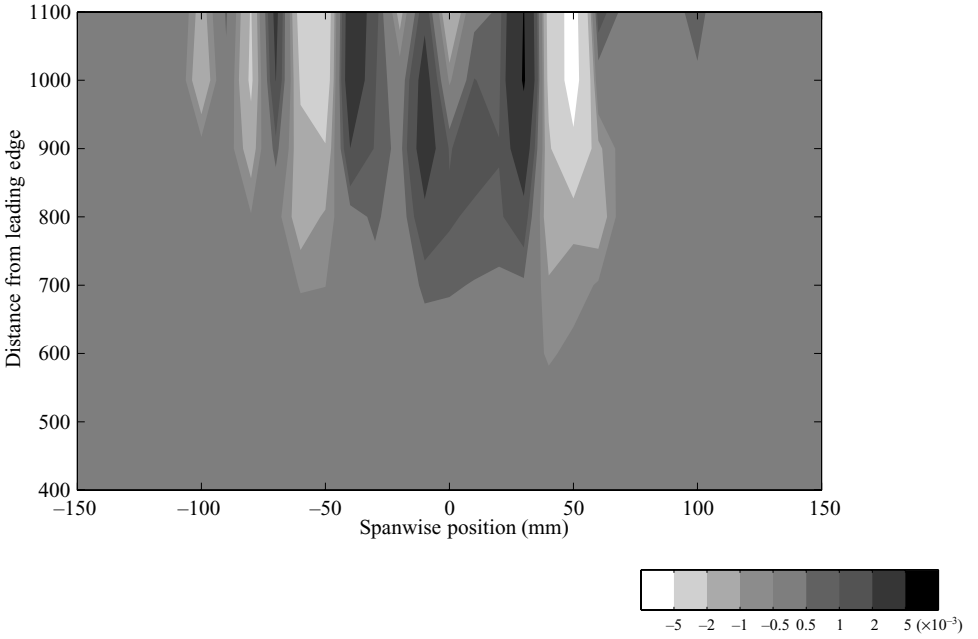


FIGURE 9. Variation of the displacement thinckess associated with the mean flow distortion, non-dimensionalized by the local theoretical displacement thickness.

Measurements at 23 other wall-normal positions were also carried out, covering a region from $y/\delta^* = 0.3$ to $y/\delta^* = 7.2$. This enabled the examinations of the mean flow distortion profiles. The procedure for extracting the distortion was to divide the velocity records in three equal parts and average the central part. This ensured that only the central amplitude-constant part of the wavetrain was considered. The shape of the distortion, not shown here, resembled that of a Klebanoff mode, with a peak inside the boundary layer. However, it appeared that the results were too noisy for a definitive conclusion to be reached.

Integrating the mean flow distortion in the wall-normal direction provided the spanwise variation of the displacement thickness associated with the streaks (figure 9). The displacement thickness variation was very small, bellow 1%. Nevertheless, it displayed a definite pattern, consistent with figure 7.

A look at the oscillating part of the signal shows other important aspects of the nonlinear regime (figure 10). This was produced by removing, from the velocity time series, the components below 15 Hz. Up to $x = 900$ mm, the picture displays the characteristic crescent shape with a central amplitude peak. At $x = 1000$ mm and $x = 1100$ mm two peaks emerge, one on each side of the centreline of the wavetrain. As is shown in § 4, this was also an outcome of nonlinear activity. The waves display significant attenuation from stations $x = 1000$ mm to $x = 1100$ mm. It appeared that the nonlinear activity was not sufficient to sustain the growth of the wavetrain very far beyond the second branch of the stability loop, which here is close to $x = 900$ mm ($Re_{\delta^*} = 1760$) (see figure 3).

In summary, it may be said that the current experiments confirmed previous findings in that the longitudinal streaks play an important role in the nonlinear evolution of this wavetrain. It also appeared that the nonlinear regime here reported could be thought of as a two-stage process. In the first stage, namely $x = 700$ mm to $x = 900$ mm,

https://doi.org/10.1017/S0022112004009188 Published online by Cambridge University Press

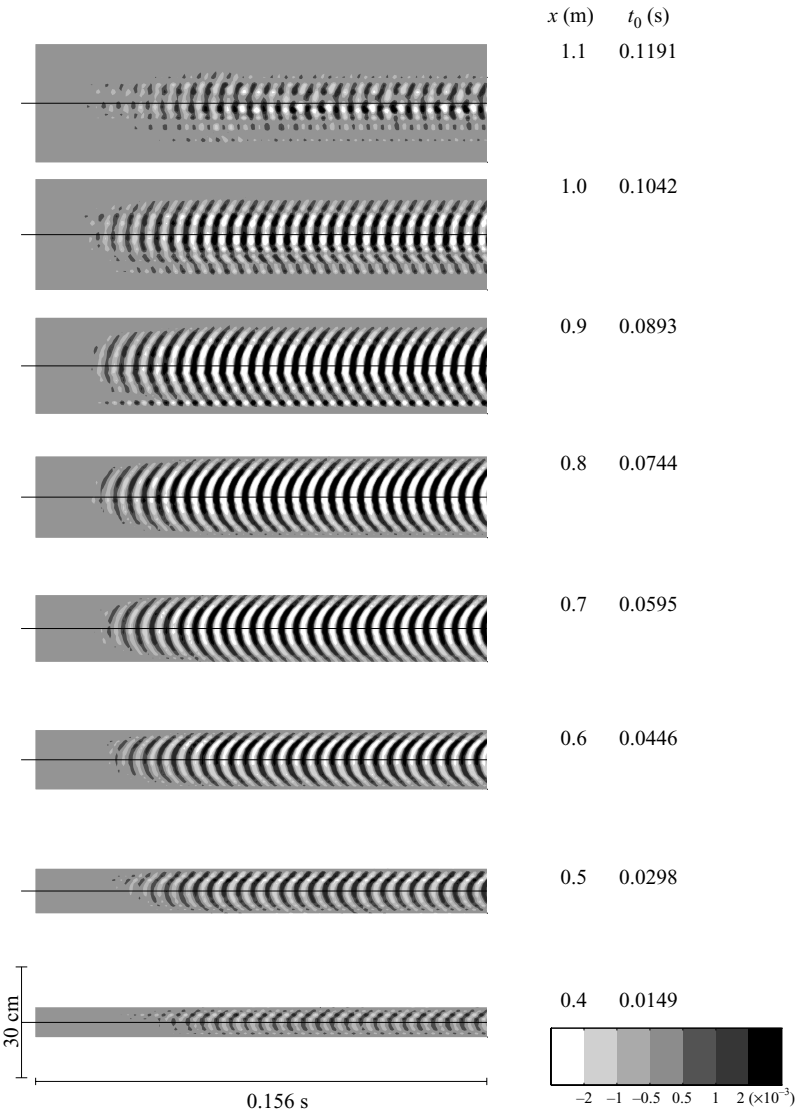


FIGURE 10. Evolution of the oscillating part of the three-dimensional wavetrain at $0.6\delta^*$ from the wall, showing the formation of the peak-and-valley structure of the streamwise velocity. The grey scale gives the velocity magnitude relative to the free-stream velocity.

the structure of the mean flow distortion was relatively simple: one negative central streak and a pair of positive streaks, one on each side of the centreline. In the second stage, $x = 1000$ mm to $x = 1100$ mm, other streaks appeared and the characteristic spanwise wavenumber increased. Also at this stage, two off-the-centreline peaks of the oscillation amplitude emerged and a valley was formed along the centreline. Hereinafter, this will be called the peak-and-valley structure and refers only to the oscillating part of the signal, as opposed to the streak structure, which describes the three-dimensional mean flow distortion and is associated with longitudinal vorticity.

The first stage was indeed similar to that reported by Stemmer *et al.* (1998), and resembled oblique transition. However, the features related to the second stage have

https://doi.org/10.1017/S0022112004009188 Published online by Cambridge University Press

not been observed in either the direct numerical simulations of Stemmer *et al.* (1998) or the various oblique transition studies. First of all, in these studies, the spanwise wavenumber of the streak structure remained constant almost until breakdown into turbulence. Moreover, no peak-and-valley structure that could be attributed to nonlinear mechanisms has been reported. These remarkable differences were here subjected to a more detailed investigation.

It is important to emphasize that the experiment reported here involved waves of very small amplitude, about ten times smaller than those used by Stemmer *et al.* (1998) and those generally used in oblique transition investigations. As has already been anticipated, this was done because the oscillations that occur in natural transition can be very small. This important aspect may be linked to the observed differences between the current investigation and other similar studies.

4. Physical model for the first stage of the nonlinear regime

In a nonlinear analysis, it is often interesting to investigate the Reynolds stresses that are neglected in the linear theory. The following derivation was inspired by that given by other studies (Benney 1961; Antar & Collins 1975; Nelson & Craik 1977) which should be used for further details. The main difference is that here a spatial evolution was considered. The flow field is expanded in a perturbation series whose small parameter, a, is a measure of the amplitude of the wave system:

$$\left.\begin{aligned} \boldsymbol{v} &= \boldsymbol{v}_0 + a\boldsymbol{v}_1 + a^2\boldsymbol{v}_2 + \ldots, \\ p &= p_0 + ap_1 + a^2 p_2 + \ldots, \end{aligned}\right\} \tag{1}$$

where $\boldsymbol{v}$ is the velocity vector with components (u, v, w) and p is the pressure. The base flow is represented by $\boldsymbol{v}_0$ and is considered parallel:

$$\boldsymbol{v}_0 = (u_0(y), 0, 0). \tag{2}$$

The order a flow is the wavetrain. If ω is the non-dimensional frequency of the excitation, $\boldsymbol{v}_1$ takes the form:

$$\left.\begin{aligned} \boldsymbol{v}_1 &= \tilde{\boldsymbol{v}}_1(x, y, z)\mathrm{e}^{\mathrm{i}\omega t} + \tilde{\boldsymbol{v}}_1^*(x, y, z)\mathrm{e}^{-\mathrm{i}\omega t}, \\ p_1 &= \tilde{p}_1(x, y, z)\mathrm{e}^{\mathrm{i}\omega t} + \tilde{p}_1^*(x, y, z)\mathrm{e}^{-\mathrm{i}\omega t}, \end{aligned}\right\} \tag{3}$$

where the asterisk denotes complex conjugate.

Substituting (1), (2) and (3) into the equations of motion for an incompressible flow and collecting terms of order a yields:

$$\left.\begin{aligned} \mathrm{i}\omega\tilde{u}_1 + u_0\frac{\partial\tilde{u}_1}{\partial x} + \tilde{v}_1\frac{\partial u_0}{\partial y} &= -\frac{\partial\tilde{p}_1}{\partial x} + \frac{1}{R_{\delta^*}}\nabla^2\tilde{u}_1, \\ \mathrm{i}\omega\tilde{v}_1 + u_0\frac{\partial\tilde{v}_1}{\partial x} &= -\frac{\partial\tilde{p}_1}{\partial y} + \frac{1}{R_{\delta^*}}\nabla^2\tilde{v}_1, \\ \mathrm{i}\omega\tilde{w}_1 + u_0\frac{\partial\tilde{w}_1}{\partial x} &= -\frac{\partial\tilde{p}_1}{\partial z} + \frac{1}{R_{\delta^*}}\nabla^2\tilde{w}_1, \\ \frac{\partial\tilde{u}_1}{\partial x} + \frac{\partial\tilde{v}_1}{\partial y} + \frac{\partial\tilde{w}_1}{\partial z} &= 0. \end{aligned}\right\} \tag{4}$$

In the equations, x, y and z represent, respectively, the streamwise, wall-normal and spanwise directions. The velocity components u, v and w also correspond to

https://doi.org/10.1017/S0022112004009188 Published online by Cambridge University Press

the streamwise, wall-normal and spanwise directions, respectively. The variables are non-dimensional. The length scale is the boundary-layer displacement thickness δ^*. The velocity scale is U_∞ and the time scale is δ^*/U_∞. R_{δ^*} is the Reynolds number based on the displacement thickness and ∇^2 is the Laplacian operator. Equations (4), with homogeneous boundary conditions, govern the linear evolution of the wavetrain and there are standard techniques for solving them (Mack 1984).

Using these techniques, the linear evolution of the wavetrain was computed considering a locally parallel flow. It was considered that the point source excited a flat spanwise wavenumber spectrum. This is, of course, only an approximation. First of all, it is not entirely clear that the excitation worked like an ideal point source. Moreover, we should consider the receptivity process, which is known to favour higher spanwise wavenumbers (Bake *et al.* 2002). However, this assumption was shown to produce very accurate results (Gaster & Grant 1975; Gaster 1975; Mack 1984, 1985). For finding a suitable amplitude, the theoretical results were matched to the experiments at $x = 700$ mm.

Results for the streamwise velocity component are given in figure 11. At $x = 400$ mm and $x = 500$ mm, the wavetrain displays amplitude peaks off the centerline. Also at $x = 400$ mm, close to the centreline, the wave system has a peculiar phase variation. Both these features have been observed in the calculations by Mack (1984, 1985). They were not detected in the experiment (figure 5), but this is probably due to poor experimental resolution and other experimental imperfections.

From $x = 600$ mm to 800 mm, agreement between experiment and theory was good, in particular when the filtered signals of figure 10 are considered. At $x = 1000$ mm and $x = 1100$ mm, the linear wavetrain displays an amplitude peak along the centreline, while the experiments clearly showed amplitude peaks off the centreline of the wavetrain. This difference was also attributed to nonlinear effects.

Figure 12 shows the linear evolution of the spanwise spectra for the three velocity components. For comparison, experimental results for the oscillating part of the streamwise velocity component are also shown. They are given as symbols connected by a solid line, and are restricted to the linear and early nonlinear stages. In the figure, the asymmetry of the experimental results appears more clearly. However, on the right-hand side of stations $x = 600$ mm and $x = 700$ mm, the agreement may be considered very good. The theoretical results show that, initially, the streamwise velocity is dominated by three-dimensional modes, but beyond $x = 900$ mm, the two-dimensional mode is the largest. The same is true of the wall-normal component, but the two-dimensional mode becomes the largest much earlier. Obviously, the spanwise velocity component is always dominated by three-dimensional modes, but the spanwise wavenumber changes significantly along the evolution. The results presented referred to the position $y = 0.6\delta^*$, but indicate the situation throughout the boundary layer.

As explained by Benney (1961), the $\boldsymbol{v}_2$ flow includes a mean flow distortion and a harmonic oscillation. It is the mean flow distortion that appears to be related to the experimental observations. The equations for the secondary mean flow distortion are:

$$u_0\frac{\partial\tilde{u}_2}{\partial x}+\tilde{v}_2\frac{\partial u_0}{\partial y}+\frac{\partial\tilde{p}_2}{\partial x}-\frac{1}{R}\nabla^2\tilde{u}_2=-2\frac{\partial}{\partial x}(\tilde{u}_1\tilde{u}_1^*)-\frac{\partial}{\partial y}(\tilde{u}_1\tilde{v}_1^*+\tilde{u}_1^*\tilde{v}_1)-\frac{\partial}{\partial z}(\tilde{u}_1\tilde{w}_1^*+\tilde{u}_1^*\tilde{w}_1), \tag{5a}$$

$$u_0\frac{\partial\tilde{v}_2}{\partial x}+\frac{\partial\tilde{p}_2}{\partial y}-\frac{1}{R}\nabla^2\tilde{v}_2=-\frac{\partial}{\partial x}(\tilde{v}_1\tilde{u}_1^*+\tilde{v}_1^*\tilde{u}_1)-2\frac{\partial}{\partial y}(\tilde{v}_1\tilde{v}_1^*)-\frac{\partial}{\partial z}(\tilde{v}_1\tilde{w}_1^*+\tilde{v}_1^*\tilde{w}_1), \tag{5b}$$

https://doi.org/10.1017/S0022112004009188 Published online by Cambridge University Press

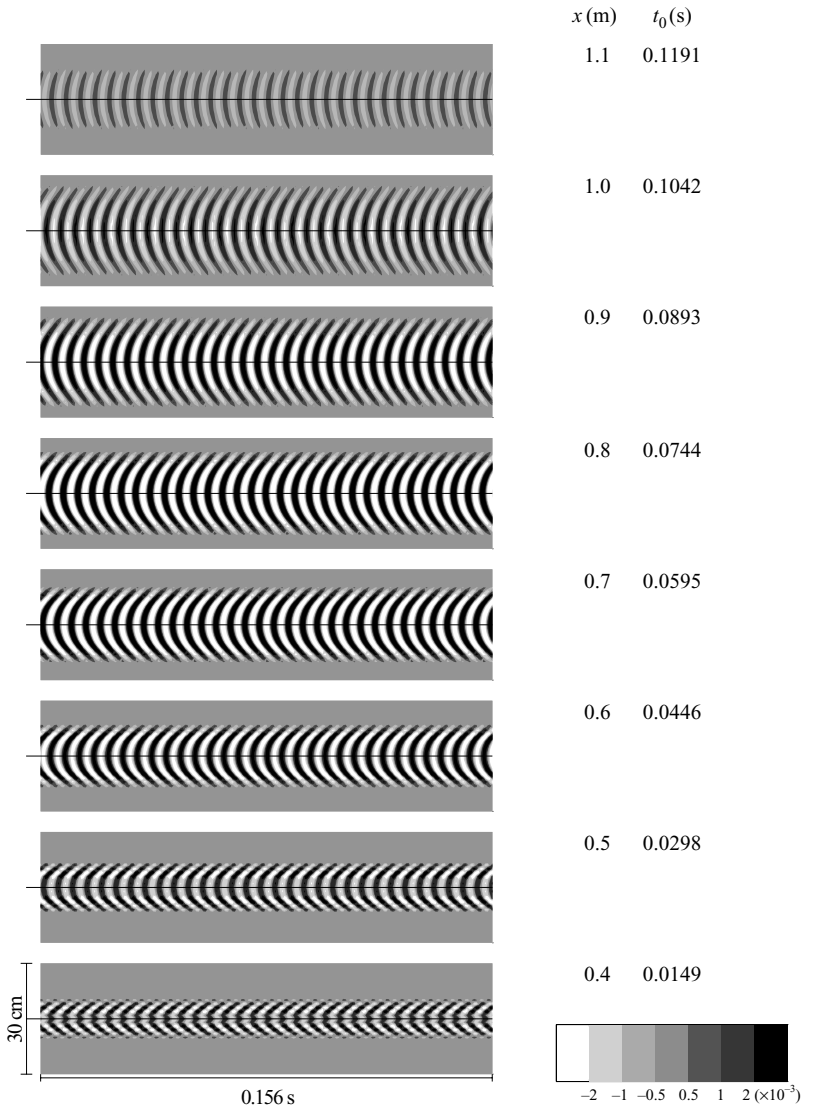


FIGURE 11. Linear stability theory results. Evolution of the streamwise velocity component at $0.6\delta^*$ from the wall shown by span × time planes. The grey scale gives the velocity magnitude relative to the free-stream velocity.

$$u_0\frac{\partial\tilde{w}_2}{\partial x}+\frac{\partial\tilde{p}_2}{\partial z}-\frac{1}{R}\nabla^2\tilde{w}_2=-\frac{\partial}{\partial x}(\tilde{w}_1\tilde{u}_1^*+\tilde{w}_1^*\tilde{u}_1)-\frac{\partial}{\partial y}(\tilde{w}_1\tilde{v}_1^*+\tilde{w}_1^*\tilde{v}_1)-2\frac{\partial}{\partial z}(\tilde{w}_1\tilde{w}_1^*),\quad(5c)$$

$$\frac{\partial\tilde{u}_2}{\partial x}+\frac{\partial\tilde{v}_2}{\partial y}+\frac{\partial\tilde{w}_2}{\partial z}=0.\quad(5d)$$

It is also interesting to consider the equation for the second-order streamwise vorticity

$$\xi_2=\frac{\partial w_2}{\partial y}-\frac{\partial v_2}{\partial z},\quad(6)$$

https://doi.org/10.1017/S0022112004009188 Published online by Cambridge University Press

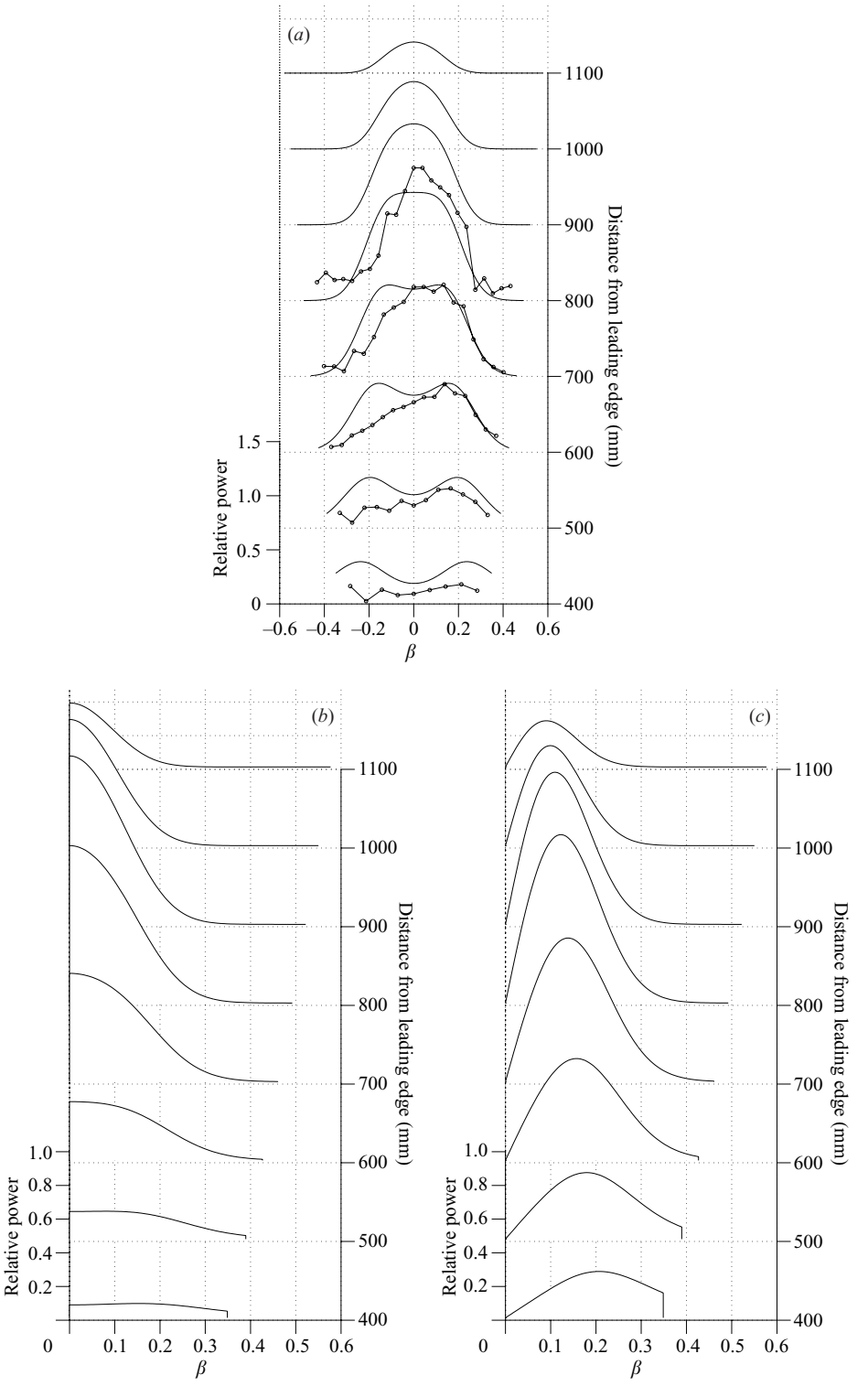


FIGURE 12. Evolution of the spanwise spectra of the three velocity components at $0.6\delta^*$ from the wall. (*a*) Streamwise, (*b*) Wall-normal and (*c*) spanwise component. The solid lines give the results from linear stability theory. For comparison, the symbols connected by a solid line give the experimental results for the oscillating part of streamwise velocity component.

https://doi.org/10.1017/S0022112004009188 Published online by Cambridge University Press

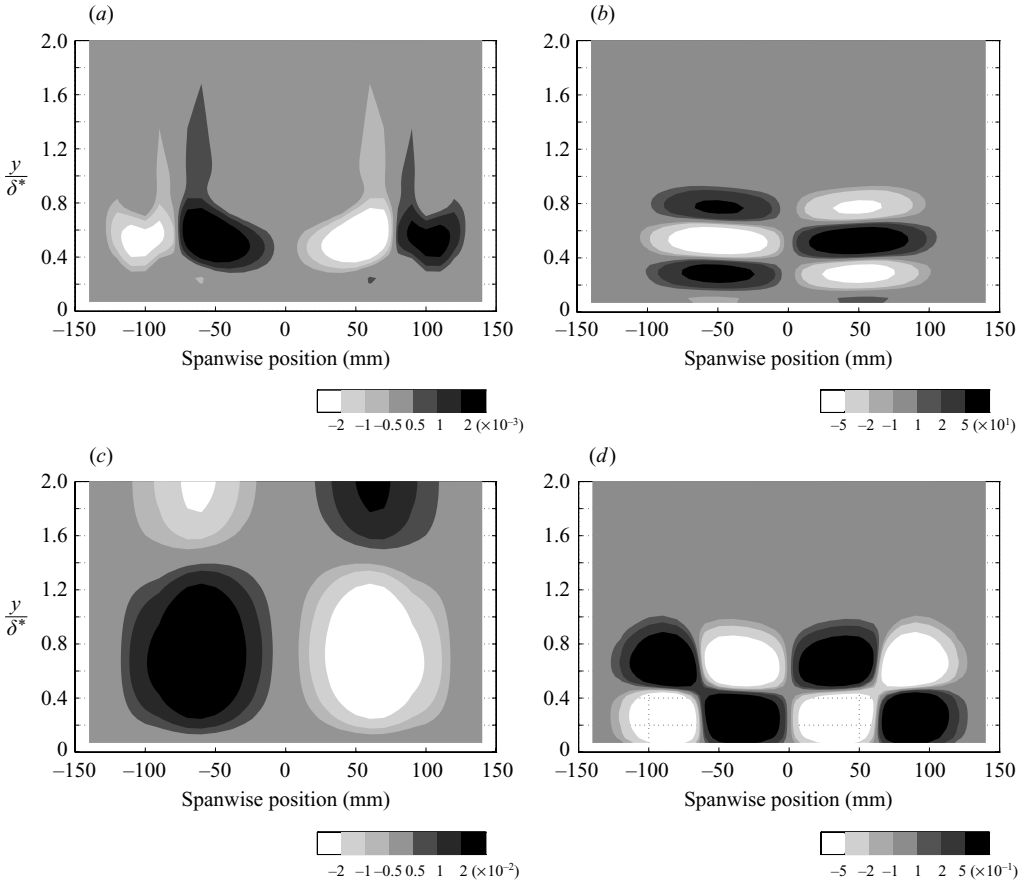


FIGURE 13. The curly bracketed non-homogeneous terms of equation (7) at $x = 800$ mm. (*a*) First term; (*b*) second term; (*c*) third term; (*d*) fourth term; The grey scale indicates the magnitude of the non-dimensional nonhomogeneous terms.

which is obtained from a combination of (5*b*) and (5*c*):

$$u_0\frac{\partial\tilde{\xi}_2}{\partial x}+\frac{\partial u_0}{\partial y}\frac{\partial\tilde{w}_2}{\partial x}-\frac{1}{R}\nabla^2\tilde{\xi}_2=\frac{\partial}{\partial x}\left[\frac{\partial}{\partial z}(\tilde{v}_1\tilde{u}_1^*+\tilde{v}_1^*\tilde{u}_1)-\frac{\partial}{\partial y}(\tilde{w}_1\tilde{u}_1^*+\tilde{w}_1^*\tilde{u}_1)\right]$$
$$+\left\{\frac{\partial^2}{\partial z^2}(\tilde{v}_1\tilde{w}_1^*+\tilde{v}_1^*\tilde{w}_1)-\frac{\partial^2}{\partial y^2}(\tilde{v}_1\tilde{w}_1^*+\tilde{v}_1^*\tilde{w}_1)+2\frac{\partial^2}{\partial z\partial y}(\tilde{v}_1\tilde{v}_1^*)-2\frac{\partial^2}{\partial z\partial y}(\tilde{w}_1\tilde{w}_1^*)\right\}. \quad (7)$$

This is a restricted version of an equation given by Elofsson & Alfredsson (1998).

Equation (5) admits solutions similar to those of (4), but must also include a particular solution due to the non-homogeneous terms. These forcing terms can be explicitly calculated from the $\boldsymbol{v}_1$ obtained using linear stability solutions.

It is perhaps more meaningful to analyse the forcing terms of (7) separately. Figure 13 shows contour plots of the four non-homogeneous terms in the curly brackets of (7). The calculations were carried out for $x = 800$ mm, where the waves attained a maximum. The second non-homogeneous term in the curly brackets is about a hundred times larger than the sum of the others, and clearly gives the dominant contribution. The non-homogeneous terms outside the curly brackets are not shown as they also were found to be negligible. The dominant character of the

https://doi.org/10.1017/S0022112004009188 Published online by Cambridge University Press

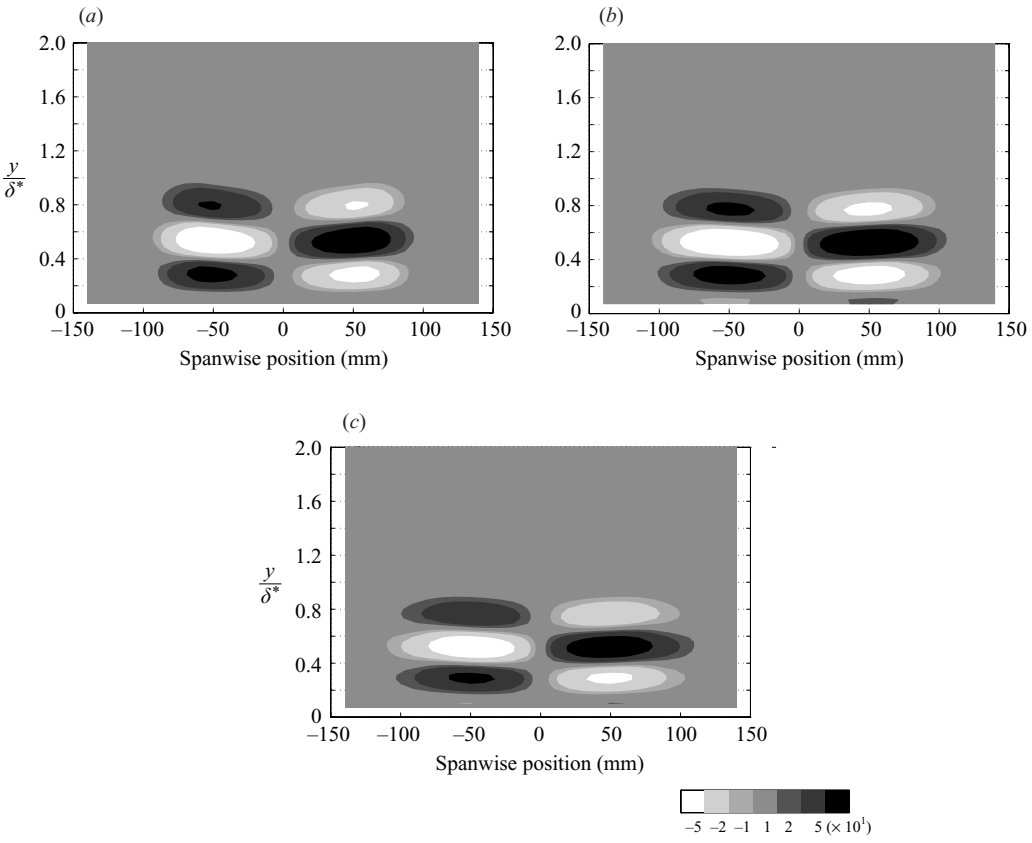


FIGURE 14. Streamwise evolution of the dominant non-homogeneous term of equation (7). (*a*) $x = 700$ mm; (*b*) $x = 900$ mm; (*c*) $x = 1000$ mm. The grey scale indicates the magnitude of the non-dimensional non-homogeneous terms.

term $-(\partial^2/\partial y^2)(\tilde{v}_1\tilde{w}_1^* + \tilde{v}_1^*\tilde{w}_1)$ is not surprising since both the experiment, figure 5, and the linear theory, figure 11, suggest that the gradients in the x- and z-directions are much smaller than those in the y-direction.

Using the arguments put forward by, for example, Benney (1961); Antar & Collins (1975) and Elofsson & Alfredsson (1998) it is clear that, owing to its symmetrical character, the dominant forcing would tend to generate two vortices of opposite sign, one on each side of the centreline. This would in turn, via transient growth, create the streak pattern observed at stations from $x = 700$ mm to $x = 900$ mm. The argument is consistent with the experimental observations.

Figure 14 gives the dominant forcing term at other stations, while figure 15 shows the evolution of its spanwise spectrum. In spite of the variation in both v and w, the forcing remains remarkably constant in shape and spectrum along the evolution. The spanwise wavenumber of the streaks should be that of the streamwise vortices. The distribution has peaks at about $\beta = \pm 0.07$ which is in good agreement with the experimental result (figure 8).

The model presented was in a way similar to that describing the nonlinear regime of oblique transition, and supports the conclusions reached by Stemmer *et al.* (1998). However, the oblique transition that has been presented in the literature (Schmid & Henningson 1992; Berlin *et al.* 1994; Elofsson & Alfredsson 1998) involves the

https://doi.org/10.1017/S0022112004009188 Published online by Cambridge University Press

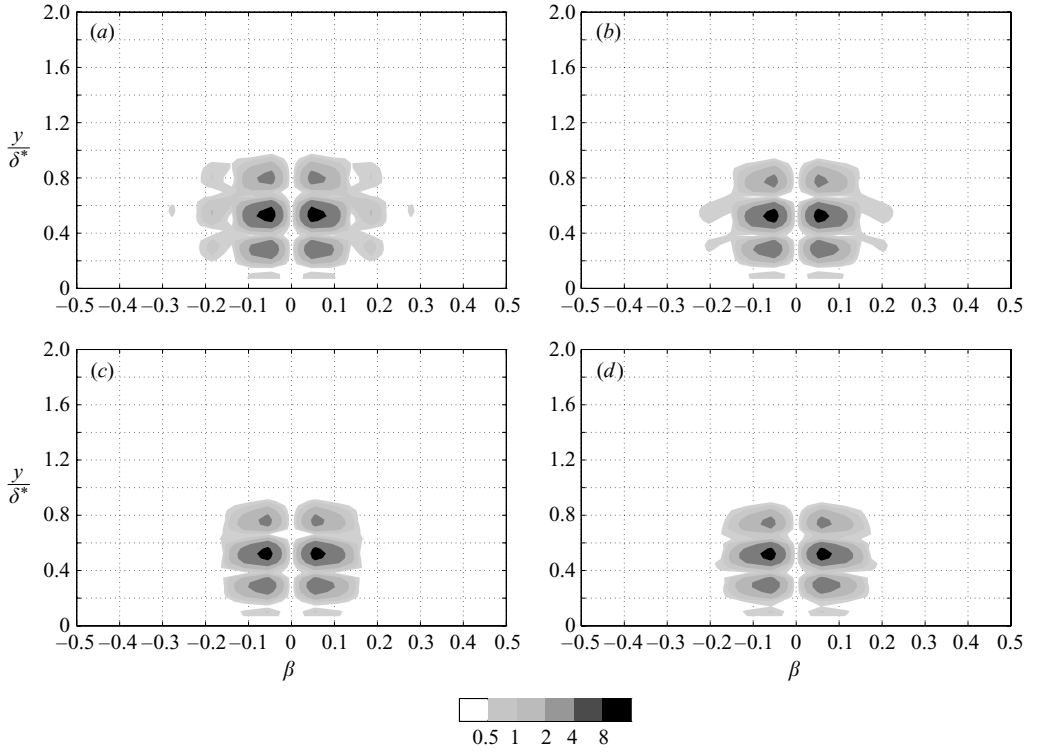


FIGURE 15. Streamwise evolution of the dominant non-homogeneous term of equation (7) in Fourier space. (*a*) $x = 700$ mm; (*b*) $x = 800$ mm; (*c*) $x = 900$ mm; (*d*) $x = 1000$ mm. The grey scale indicates relative power.

interaction of only a pair of oblique waves. Here, the interaction involves a large number of waves, including a relatively large two-dimensional wave for the v component (figure 12). The interacting waves do not have an identical phase speed, and therefore the mechanism can display dispersive features. If the modes composing v and w were sufficiently concentrated and different in spanwise wavenumber, the forcing could in fact, exhibit beating. This would be associated with a change in the sign of the forcing as it evolves in the streamwise direction. Figures 14 and 15 show that, in the current experiment, such dispersive effects were not relevant at least up to $x = 1000$ mm, where the forcing is already very weak. It should, however, be emphasized that under other circumstances, say, other Reynolds number or pressure gradient, these effects may become important. Because of these important differences, it is perhaps not appropriate to use the term oblique transition to describe the current phenomenon.

5. Search for a physical model for the second stage of the nonlinear regime

5.1. *Weakly nonlinear models*

At $x = 1000$ mm, the experiments showed a more complicated spanwise structure of the streaks. At the centre, the structure is consistent with the existence of two pairs of counter-rotating streamwise vortices. In fact, figure 13 shows that the second largest forcing term in (7) would tend to generate two pairs of counter-rotating streamwise

https://doi.org/10.1017/S0022112004009188 Published online by Cambridge University Press

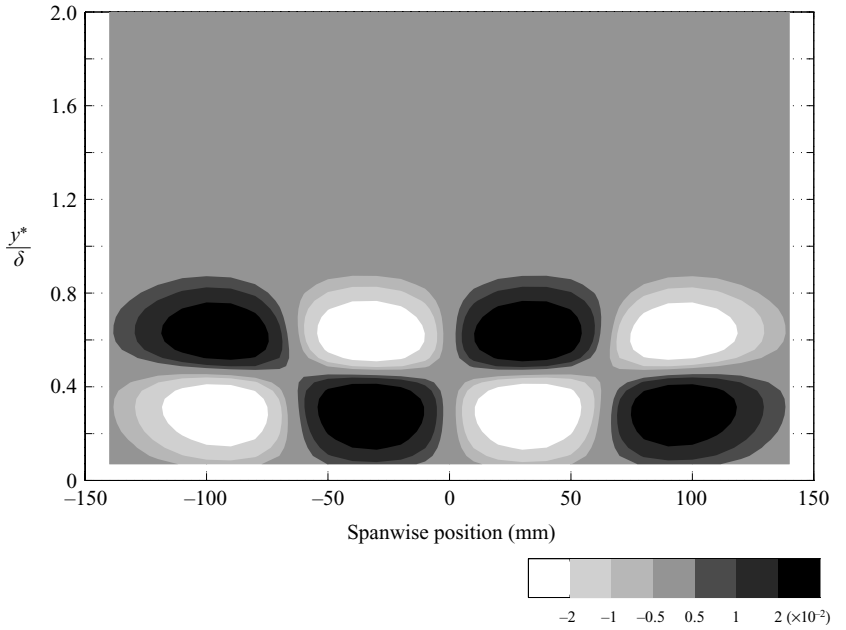


FIGURE 16. The second dominant non-homogeneous term of equation (7) at station $x = 1000$ mm. The grey scale indicates the magnitude of the non-dimensional non-homogeneous terms.

vortices, one pair at each side of the centreline. This non-homogeneous term arose from the $w_1 - w_1$ interaction. It appeared that this interaction should be further investigated.

Figure 16 shows the distribution of this forcing term at $x = 1000$ mm. The smaller magnitude of this forcing term as compared to that associated with the first nonlinear stage, figure 14, was consistent with the fact that this stage started further downstream. On the other hand, it was not consistent with the experimental observation that the streaks of the second nonlinear stage became dominant at $x = 1000$ mm and 1100 mm.

Figure 17 gives the spectral distribution. The dominant spanwise wavenumber of the forcing term is about $\beta = 0.1$. Clearly, it was not in agreement with the experimental values of 0.2, 0.3 and 0.4.

Yet another argument could be raised to confirm that this forcing term could not be held responsible for the second stage of the nonlinear regime. In studying nonlinear regimes, it is sometimes helpful to check the amplitude scaling of the nonlinear phenomenon. This scaling can be obtained from experiments along the centreline of the plate. An experiment was then carried out with this purpose. Five different amplitude levels were tested. The length of the wavetrain was identical to that of figure 1, as were the free-stream velocity and other relevant parameters. To extract the mean flow distortion along the centreline of the wavetrain, the procedure was identical to that adopted in producing figure 9, namely, to divide the velocity records into three equal parts and average the central part.

For the streamwise stations from $x = 700$ mm to 1100 mm, the amplitude of the mean flow distortion was plotted against the square of the amplitude of the fundamental wave at $x = 600$ mm (figure 18). At stations $x = 700$ mm to $x = 900$ mm, the distortion is negative. The largest absolute value is found at $x = 800$ mm. For $x = 1000$ mm and

https://doi.org/10.1017/S0022112004009188 Published online by Cambridge University Press

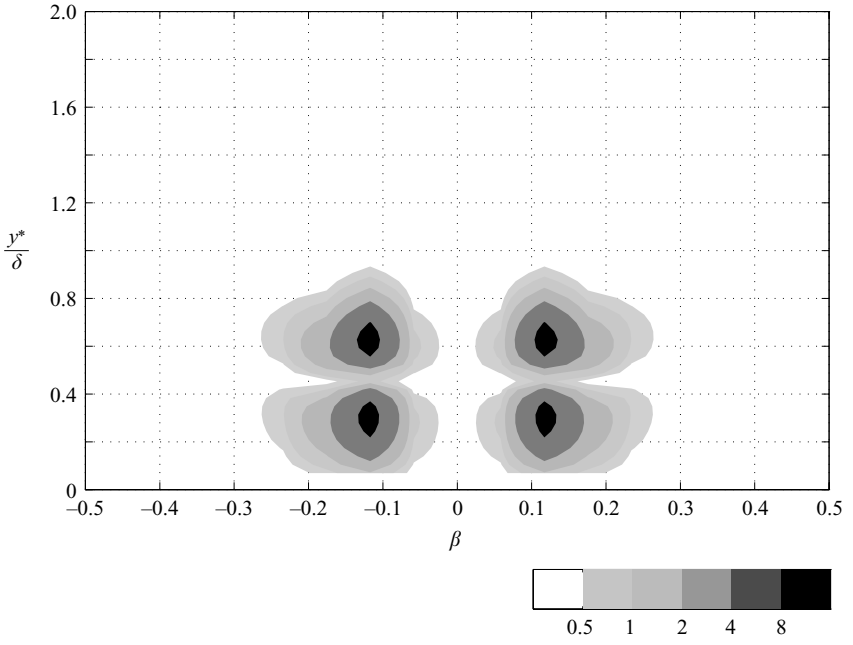


FIGURE 17. The second dominant non-homogeneous term of equation (7) at station $x = 1000$ mm. Fourier space. The grey scale indicates relative power.

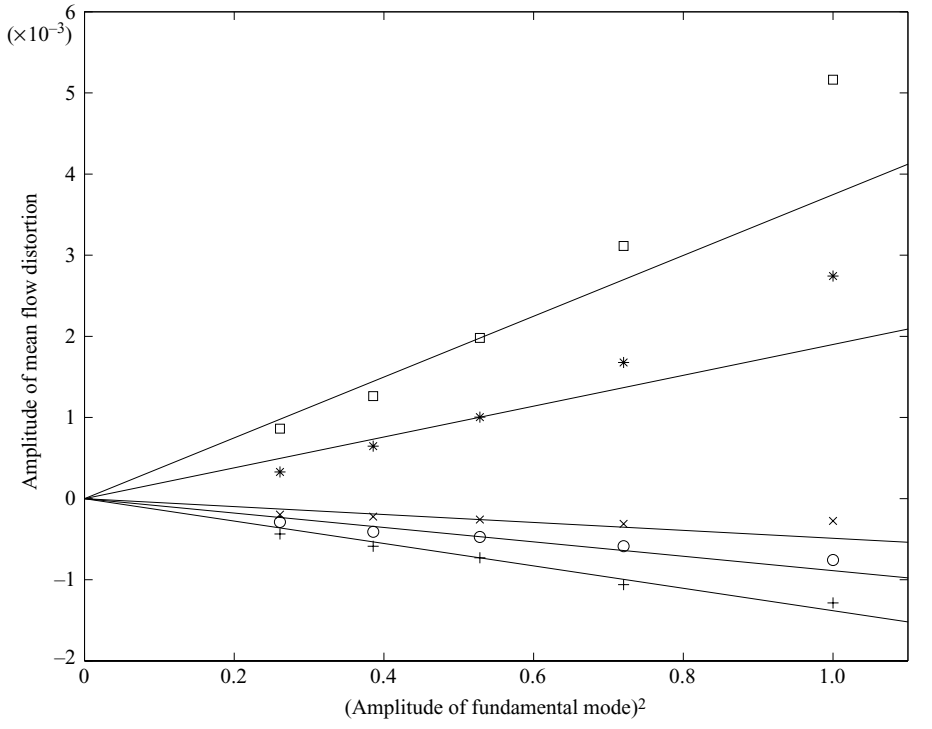


FIGURE 18. The scaling of the mean flow distortion relative to the wave amplitude. The symbols ×, ○, +, * and □ correspond to stations from 700 mm to 1100 mm, respectively.

https://doi.org/10.1017/S0022112004009188 Published online by Cambridge University Press

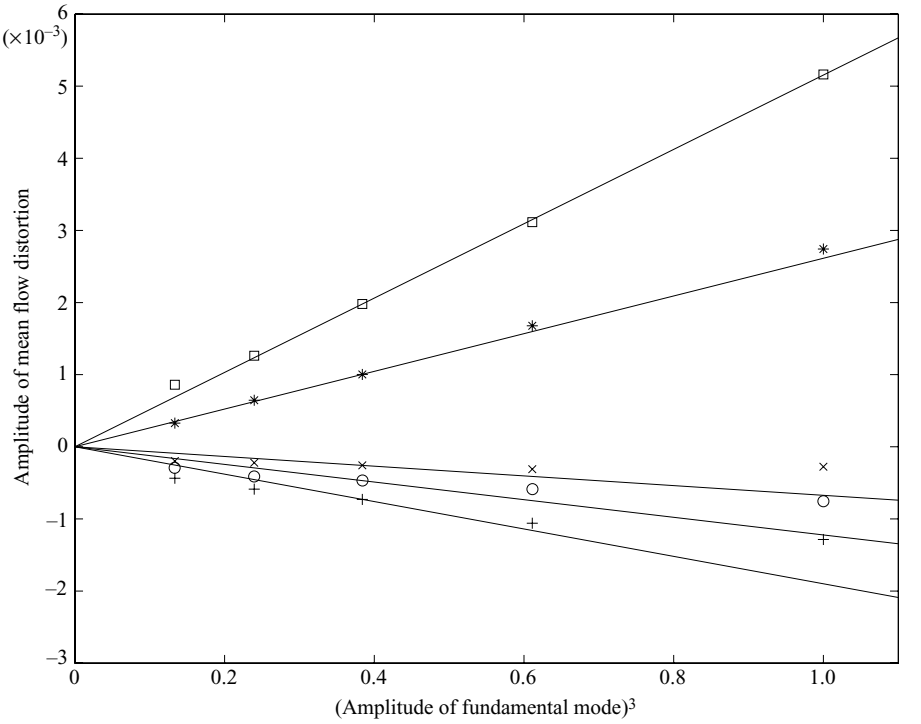


FIGURE 19. The scaling of the mean flow distortion relative to the wave amplitude. Symbols as for figure 18.

$x = 1100$ mm, the distortion is positive. In the figure, five straight lines are also given that cross the origin and the mean value of each set of experimental results. The agreement in the first stage of the nonlinear regime is very good, offering further confirmation of the conclusions reached in the previous section. However, for the second stage of the nonlinear regime, namely, stations $x = 1000$ mm and 1100 mm, the mean flow distortion clearly scales to a higher than second power of the amplitude. The result lent further support to the conclusion that this stage was not associated with the $w_1 - w_1$ interaction.

Figure 19 gives the mean flow distortion along the centreline against the third power of the wave amplitude. The agreement in the second nonlinear stage, $x = 1000$ mm and 1100 mm, is good. The analysis is consistent considering that at these stations the a^2 effect of the first nonlinear stage is relatively small, as indicated by figure 8.

The result pointed to the possibility that the phenomenon was linked to a higher-order nonlinear correction. It is known that such corrections are proportional to increasing powers of the fundamental wave amplitude (Stuart 1960). Therefore, this possibility was also investigated.

From figure 8, it can be seen that the energy of the modes in the second stage of the nonlinear regime is larger than that of the first stage. If a is small, the a^3 correction would have to be smaller than an a^2 one. This was not consistent with the experiments. Moreover, in such a model, the higher correction would have to be a harmonic of the lower ones. In the current experiment, the argument would lead to a wavenumber of 0.14. This also was not in agreement with the experimental results (figure 8) which exhibited wavenumbers of 0.2, 0.3 and 0.4.

https://doi.org/10.1017/S0022112004009188 Published online by Cambridge University Press

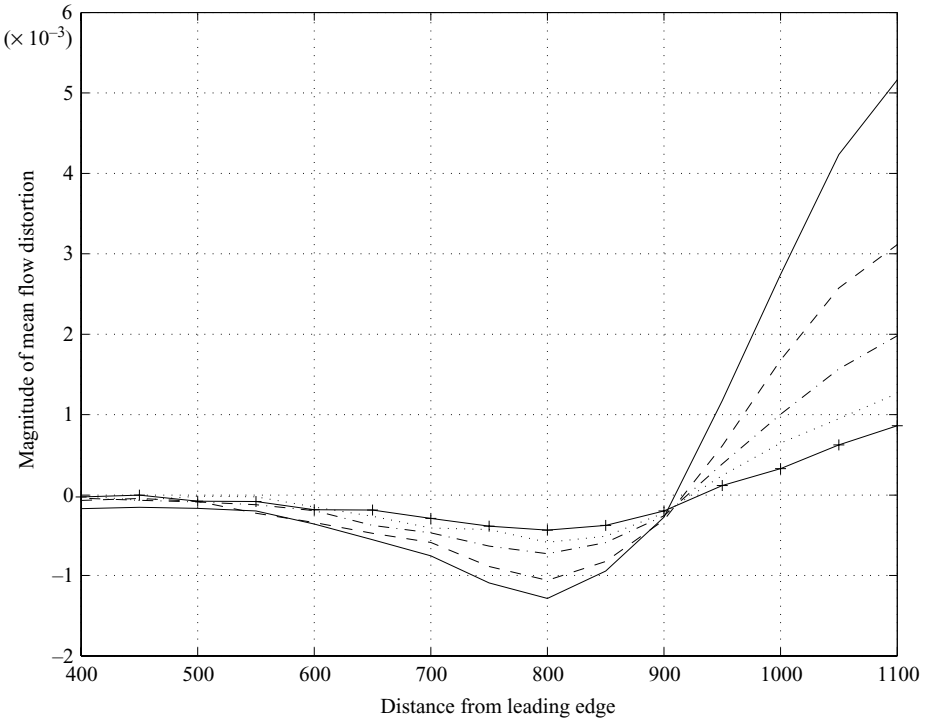


FIGURE 20. Centreline evolution of the mean distortion for different wave amplitudes.

Yet, a perhaps stronger argument could be raised. Figure 20 presents, in a different way, the same data as used in figures 18 and 19. Here, the downstream evolution of the mean flow distortion along the centreline for different wave amplitudes is shown. In a weakly nonlinear framework, the importance of higher-order effects depends on the wave amplitude. As the wave amplitude is increased, the higher-order effects have to move closer to the excitation source. Figure 20 clearly shows that the distortion reaches a saturation at $x = 800$ mm, regardless of the wave amplitude. Based on these arguments, it was concluded that this model also could not be associated with the experimental observations.

In fact, if the second stage of the nonlinear regime here reported was a consequence of a higher-order weakly nonlinear interaction, it should have also appeared in the numerical simulation reported by Stemmer *et al.* (1998), which involved higher wave amplitudes. They would probably also have been observed in some of the many investigations of oblique transition.

5.2. *A secondary instability model*

Another shortcoming of the weakly nonlinear models described above in connection with the second nonlinear stage was that neither of them had anything to say about the nonlinear peak-and-valley structure of the oscillating part of the signal, which also appeared in this stage (figure 10). It then seemed appropriate to verify whether this structure was in some way linked to the streak structure of the mean flow distortion.

Further insight into the simultaneous evolution of the peak-and-valley structure and the mean flow distortion could be gained by comparing the signals in Fourier space. Figure 21 shows the spanwise spectra of both the oscillating and the mean parts of the signal. For comparison, predictions from linear stability theory are also

https://doi.org/10.1017/S0022112004009188 Published online by Cambridge University Press

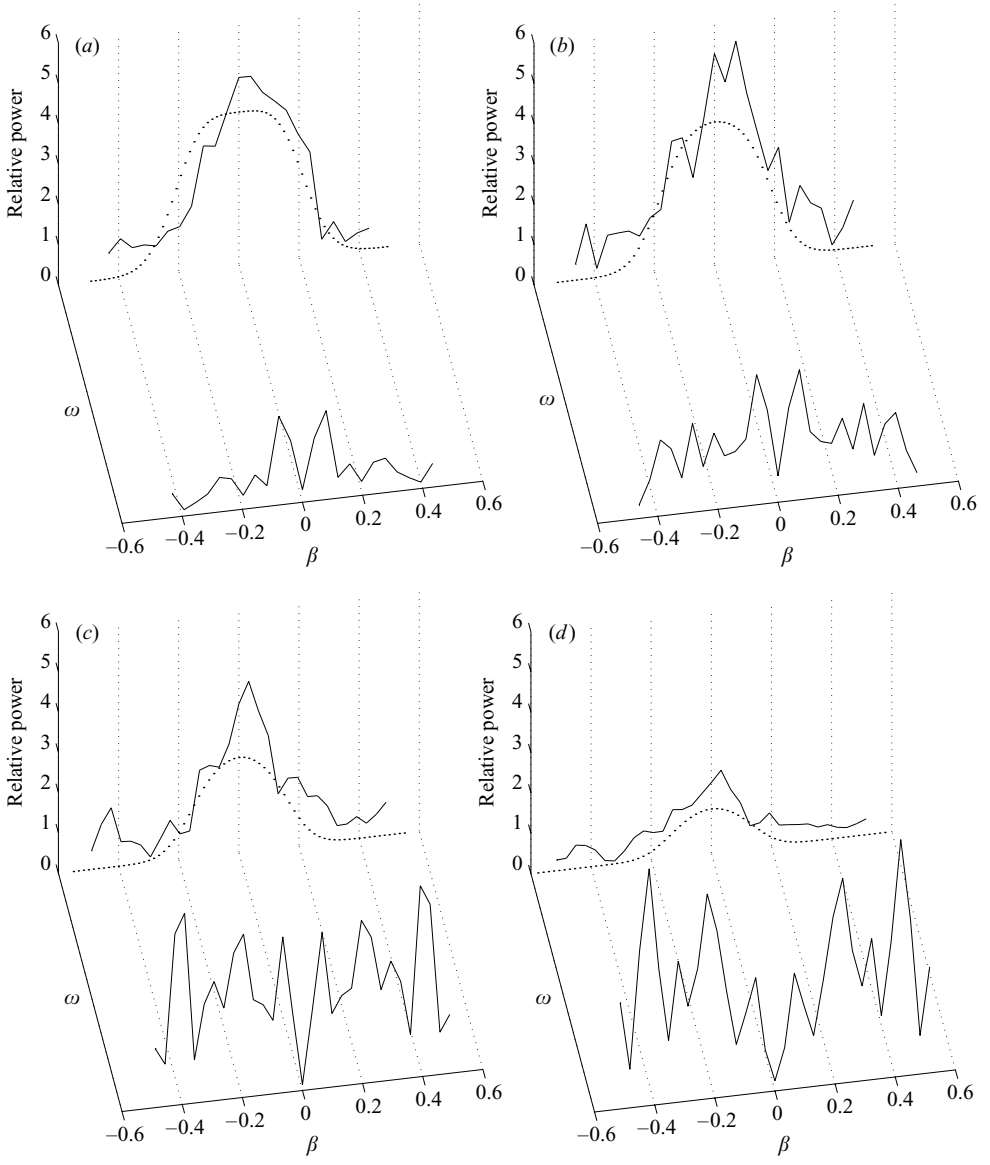


FIGURE 21. Spanwise spectra for stations (*a*) $x = 800$ mm, (*b*) 900 mm, (*c*) 1000 mm and (*d*) 1100 mm. The oscillating signal is given by the solid line at the back and compared to predictions from linear stability theory (dotted lines). The mean flow distortion is represented by the line at the front.

given as dotted lines. At $x = 800$ mm, the spectral distribution of the oscillating part of the signal is relatively smooth. It is not very symmetrical and is also noisy, but these were attributed to experimental imperfections. At this station, the three-dimensional mean flow distortion displays essentially the two peaks, $\beta = \pm 0.07$, investigated in § 4. At $x = 900$ mm and beyond, both the oscillating part and the mean flow distortion developed other spectral peaks.

The peak-and-valley structure and the selective growth of three-dimensional waves of the fundamental frequency pointed to a secondary instability of the Klebanoff

https://doi.org/10.1017/S0022112004009188 Published online by Cambridge University Press

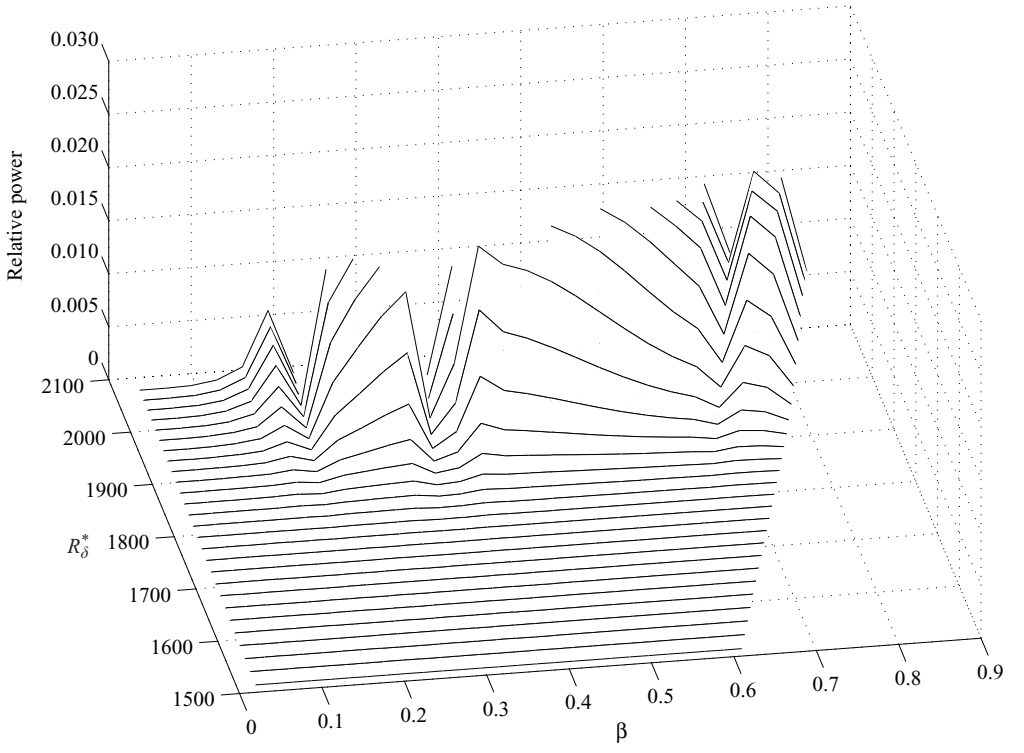


FIGURE 22. Results from PSE calculations. The downstream evolution of the three-dimensional modes under fundamental resonance.

type, whereby three-dimensional waves are amplified by fundamental resonance. In this instability, while the peak-and-valley structure is formed, a streak structure also develops. The mechanism of formation of this three-dimensional mean flow distortion was described by Benney (1961). It involves the nonlinear generation of longitudinal vortices and transient growth of streaks.

To check the argument, a number of parabolized stability equation (PSE) simulations were carried out. Each time, the boundary layer was excited with only a pair of three-dimensional waves and a two-dimensional wave of identical frequency. The amplitude of the two-dimensional wave was matched to the amplitude of the wavetrain at $x = 800\,\text{mm}$ on the centreline. Three-dimensional modes were excited at an amplitude of 10^{-6} relative to the free-stream velocity. The different spanwise wavenumbers used covered the range 0 to 0.6 at the inflow boundary condition of the simulations, namely, $R_{\delta^*} = 1500$.

Figure 22 displays the downstream evolution of the three-dimensional modes under fundamental resonance as obtained from the PSE computations. It is not the simultaneous evolution of all three-dimensional modes composing the wavetrain. It is the evolution of a number of pairs of three-dimensional waves subjected to fundamental resonance, each pair simulated separately, but the results collected together in one picture. Figure 23 shows the evolution of the mean flow distortion arising from the Reynolds stress interaction between the two-dimensional and the three-dimensional resonating waves. Clearly the mechanism provides a means for the selective amplification of waves and formation of streaks with spanwise wavenumbers around 0.2, 0.3, 0.4 and 0.7. Wavenumbers from 0.2 to 0.4 are in good agreement

https://doi.org/10.1017/S0022112004009188 Published online by Cambridge University Press

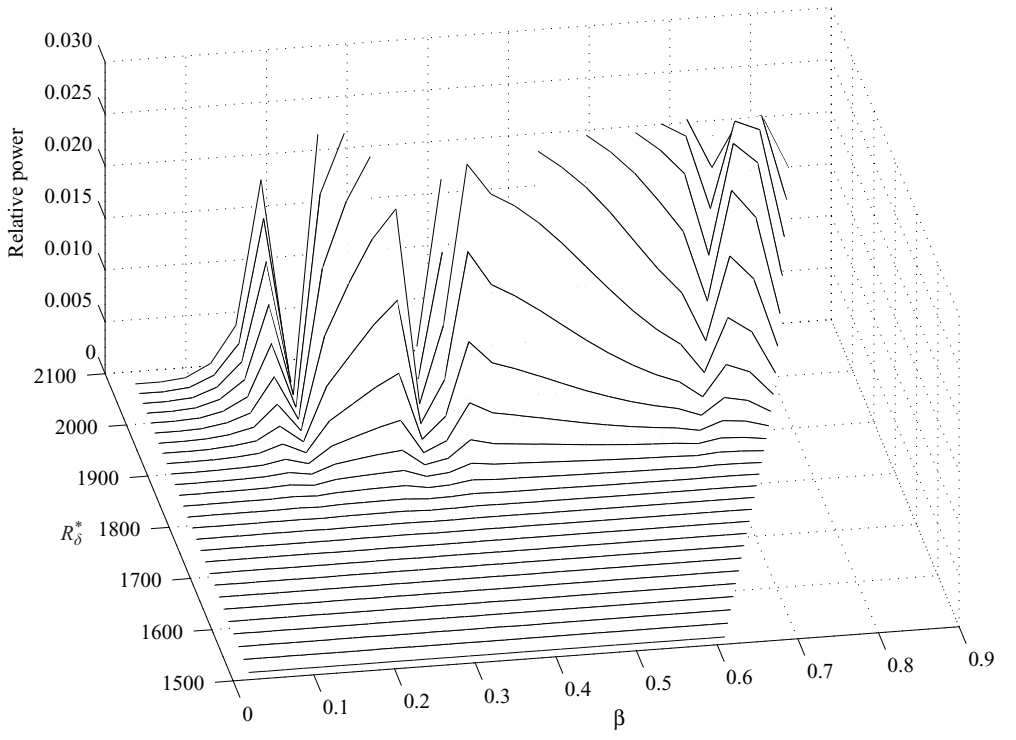


FIGURE 23. Results from PSE calculations. The downstream evolution of the three-dimensional mean flow distortion associated with the fundamental resonance.

with the experimental results. The wavenumber 0.7 is above the experimental spectral domain. Note that the amplitude of the mean flow distortion is significantly larger than that of the three-dimensional waves. This is also the case in the experiment and might explain the fact that the spectra for the streak structure are clearer than those of the peak-and-valley structure.

If the two-dimensional wave is large enough, the Klebanoff instability can lead to a self-sustained nonlinear growth of the waves, otherwise they eventually decay (Herbert 1988). Indeed, the results show that the oscillations are larger than the linear stability predictions. However, it appears that here the nonlinear activity was not strong enough to sustain the growth under the influence of the stabilizing effects of the linear stability. This is plausible considering that the fundamental waves of the current experiment have very small amplitude, well bellow the amplitudes that lead to turbulence under Klebanoff-type instability (Kachanov 1994).

In the simulations, the nonlinear activity was stronger than in the experiment and sustained the growth of the waves throughout the computational domain. However, it should be recalled that the amplitude of the two-dimensional wave of the PSE calculations was matched to the amplitude of the experimental wavetrain at station $x = 800$ mm on the centreline. Since, in the experiment, the wavetrain is three-dimensional, it is likely that the effective two-dimensional wave driving the resonance was considerably smaller than that used in the simulations. Moreover, the growth rate of the fundamental two-dimensional wave is larger than that of the three-dimensional wavetrain emanating from the point source. Also, the amplitude of the seeds for the resonating three-dimensional modes probably did not match those

https://doi.org/10.1017/S0022112004009188 Published online by Cambridge University Press

of the experiment. Apparently, there is no easy way of obtaining both the effective amplitude of the driving two-dimensional wave and of the three-dimensional seeds, and this was not attempted here. In fact, the interest did not lie in reproducing the amplitudes accurately, but in finding the most unstable three-dimensional waves. Indeed, the most unstable wavenumbers of the secondary instability were in close agreement with the experimental results. This was considered to be strong evidence that the peak-and-valley structure was linked to the mean flow distortion and that the second nonlinear stage was the outcome of a Klebanoff-type instability.

The secondary instability is strongly dependent on the amplitude of the two-dimensional driving wave. In an experiment, increasing the amplitude of the two-dimensional wave usually moves upstream the onset of secondary instability. The current experiments showed the remarkable feature that the onset of the secondary instability was not dependent on the amplitude of the driving wave. However, it must be recalled that the seeds of the three-dimensional waves also play a role in triggering the secondary instability, and it was decided to investigate the origin of these seeds.

The seeds of the three-dimensional resonating modes may come from the background non-deterministic noise. However, the repeatability of the experiment, shown by the standard deviation in figure 6, made it clear that the seeds had to be deterministic. Indeed the point-source excitation contained modes of the correct frequency for the resonance to develop. However, the streamwise velocity component of the three-dimensional waves excited at the source had a peak at the centreline $z = 0$. They would have to produce a peak-and-valley structure with a peak at $z = 0$, not a valley, as observed in the experiment.

The explanation that was eventually found was also inspired by Klebanoff's experiment (Klebanoff *et al.* 1962). In that experiment, the three-dimensionality was artificially introduced by the placement of spacers under the vibrating ribbon. The appearance of three-dimensionality in the nominally two-dimensional wavetrain was attributed to spanwise modulation of the linear amplification owing to spanwise variation of the Reynolds number based on the displacement thickness. The argument was that the spacers produced small defects in the boundary-layer profile which yielded a variation across the span of the displacement thicknesses. At the spacer positions, larger displacement thicknesses were produced and hence higher Reynolds number. As a consequence, close to the first branch, larger amplification rates were expected at the spacer positions, and accordingly peaks should develop. On the other hand, close to the second branch, valleys should appear at the spacer locations. In that experiment, the spanwise variation of the displacement thickness was not measured, as it was estimated to be below the experimental uncertainty of 1%. Nevertheless, the argument was confirmed by the experimental results which showed the expected phase shift. This is clearly displayed in figure 13 of Klebanoff *et al.* (1962).

In the current experiment, there were no spacers. However, at $x = 800$ mm, there was spanwise variation of displacement thickness. The variation was very small, but, as shown by Klebanoff, they need not be large. The three-dimensionality thus generated could provide the seeds for the subsequent fundamental resonance. The three-dimensional seeds also need not be large. In the simulations that produced figures 22 and 23, the amplitude of the three-dimensional seeds were about 10^{-6} relative to the free-stream velocity, and under the resonant interaction, reached amplitudes comparable to those of the fundamental two-dimensional wave. In the current experiment, because of the proximity to the second branch, higher amplification rates would be expected where the displacement thickness variation was negative, and lower where positive. The variation of displacement thickness

https://doi.org/10.1017/S0022112004009188 Published online by Cambridge University Press

shown in figure 9 is consistent with the appearance of an amplitude valley at the centreline, figure 10.

This physical model also offered an explanation for the location of the onset of the secondary instability at about $x = 800$ mm, regardless of the wave amplitude. The argument is that, because of the way they are produced, the three-dimensional seeds that evolved into resonance only became available close to the second branch of the instability loop, that is, around $x = 800$ mm. Moreover, the mean flow distortion at $x = 1000$ mm and beyond would be the nonlinear outcome of an already nonlinear process. Clearly, it had to scale to a higher than second power of the wave amplitude, in agreement with figure 18.

In conclusion, it can be said that the model that associated fundamental instability with the effects related to the second branch of the stability loop was able to predict with reasonable accuracy the spanwise wavenumber of the three-dimensional structures of the second stage of the nonlinear regime. It also offered explanations for the phase, the scaling power and the fixed streamwise location of the onset of the second nonlinear stage and was consistent with the deterministic character of the experimental results. Based on these results, it was concluded that this was a plausible model for the second stage of the nonlinear regime.

It is important to note that other studies of wavetrains emanating from point sources (Stemmer *et al.* 1998), have not attributed any importance to either the fundamental instability or the second branch of the instability loop. However, in those studies, the disturbance amplitude was considerably higher than that used here, and turbulence occurred well before the second branch.

6. Summary and final remarks

The paper reports on an investigation of the nonlinear evolution of a wavetrain emanating from a point source in a boundary layer. It confirms previous studies in that mean flow distortions in the form of longitudinal streaks play an important role in the process. It appeared that the streaks arise from transient growth promoted by streamwise vortices. The results suggested that the nonlinear regime under study could be thought of as a two-stage process. A physical model was proposed for each nonlinear stage.

In the first stage, the streaks displayed a relatively simple pattern, with a negative central streak and one positive streak at each side of the centreline of the wavetrain. The mean flow distortion scaled to the second power of the wave amplitude. For this stage, a weakly nonlinear model was presented. The model involved a Reynolds-stress interaction of the spanwise and the wall-normal velocity components which was found to be dominant. It produced a pair of longitudinal vortices which are known to promote the algebraic growth of streaks via the lift-up mechanism. The spanwise wavenumber of the streaks in the first nonlinear stage was predicted well by the model, which was also consistent with the scaling power observed experimentally.

In some aspects, this stage resembled the nonlinear regime of oblique transition. However, the interaction involved not only a pair of oblique waves, but a large number of waves, including a relatively large two-dimensional one. The interacting waves do not have an identical phase speed and therefore dispersive effects can be important. Because of these important differences, it is perhaps not appropriate to regard this phenomenon as oblique transition.

In the second stage of the nonlinear regime, the negative central streak was split into two, and new streaks were formed at the edges of the wavetrain. Here, the mean flow

https://doi.org/10.1017/S0022112004009188 Published online by Cambridge University Press

distortion scaled better to the third power of the wave amplitude. At the same time, the oscillating part of the signal displayed a peak-and-valley structure. Comparison with the linear stability calculations, also given in the paper, led to the conclusion that this peak-and-valley structure was also the outcome of nonlinear activity. A remarkable feature was that the position of the onset of the second nonlinear stage was not affected by the amplitude of the wave.

Two weakly nonlinear models have been investigated in an attempt to describe the experimental observations. They have not been able to predict many features of the second nonlinear stage. In particular, the peak-and-valley structure of the oscillating part of the signal and the fixed position of the onset of the second nonlinear stage could not be explained and these models were discarded.

A secondary instability model was then considered. It linked the peak-and-valley structure to a secondary instability of the fundamental type. PSE computations revealed that the spanwise wavenumbers of the most unstable modes were in reasonable agreement with the experiments. In the model, the streak structure of the mean flow distortion of the second nonlinear stage was associated with a nonlinear interaction similar to that of the first stage. The agreement in spanwise wavenumbers was good and the scaling power was consistent.

The deterministic character of the streak pattern made it clear that the seeds for the resonating oblique modes could not have come from the non-deterministic background noise. On the other hand, they could not have come directly from the excitation because this would not be consistent with the phase of both the peak-and-valley and the streak structures. The explanation eventually suggested was that the resonating seeds had arisen from spanwise variation of amplification rates, owing to variation of the local displacement thickness Reynolds number. This variation was caused by the mean flow distortion of the first stage of the nonlinear regime. Because of the proximity to the second branch of the linear stability loop, three-dimensional seeds thus generated would develop an amplitude valley on the centreline and peaks off the centreline, which was in agreement with the experimental observations. The argument also offered an explanation for the fixed location of the onset of the second stage of the nonlinear regime, which in the current experiment was at about $x = 800$ mm. Indeed, that is the region where the seeds would be produced by the mechanism described above.

In conclusion, it can be said that the models proposed for the first and second nonlinear stages were able to predict with reasonable accuracy the spanwise wavenumbers of the three-dimensional structures. They were also consistent with the scaling powers of the mean flow distortions observed experimentally. The model proposed for the second nonlinear stage was consistent with the deterministic character of the phenomenon investigated and offered an explanation to the phase of both the peak-and-valley structure and the streak structure. It also offered a explanation for the fixed streamwise position of the onset of the second nonlinear stage.

It would be interesting to confirm these findings via some kind of numerical simulation, but cannot be done with the parabolized stability approach used in this study. The PSE model cannot handle the modulation of the amplification rates owing to variation of Reynolds number across the span.

As reported by Klebanoff & Tidstrom (1959) and Klebanoff *et al.* (1962), early experiments revealed that natural transition usually occurs shortly after the waves cross the second branch of the stability loop. This may be linked to the arguments presented here. Apart from natural transition, other complicated scenarios such as

https://doi.org/10.1017/S0022112004009188 Published online by Cambridge University Press

the wavepacket (Medeiros & Gaster, 1999*a*, *b*) and the interaction of a point source wavetrain with the background noise (Gaster 1990) display features that have not yet been entirely explained. Perhaps some of these features are linked to the current results. Indeed, this seems to be the case for the wavepackets, and this possibility is now being investigated (Medeiros 2001).

Studying the evolution of three-dimensional wavetrains with other frequencies would provide a clearer picture of the role of the second branch. If the second branch does play a role in natural transition in boundary layers, investigation of the evolution of three-dimensional wavetrains in a parallel flow, such as the flat-plate Poiseuille flow, could shed further light onto the phenomenon. Since there the transition evolves at a constant Reynolds number, the proximity to the second branch can be used as a control parameter and a clearer picture may emerge. This investigation is also currently under way.

The wavetrain from a point source exhibited nonlinear behaviour that is characteristic of transition driven by either two-dimensional or three-dimensional waves. This is perhaps not surprising, since it is a three-dimensional wave system dominated by waves of low spanwise wavenumber. In fact, the work on boundary-layer transition has concentrated on the evolution of monochromatic plane wavetrains. Underlying this approach, there was always the expectation that such studies would afford an explanation for the more complicated scenario of natural transition. This expectation has, at least partially, been fulfilled by the observation of growth of subharmonic waves (Shaikh 1997) and the formation of streaks (Westin *et al.* 1994) in natural transition. The current paper gives further confirmation of the usefulness of this approach. It is expected that these results will help further work in natural transition.

The author acknowledges the fruitful discussions with Dr M. Mendonça, who also performed the PSE computations. Discussions with Professor M. Gaster, who provided the Orr–Sommerfeld code, and Professor P. Monkewitz are also acknowledged.

REFERENCES

Antar, B. N. & Collins, F. G. 1975 Numerical calculations of finite amplitude effects in unstable laminar boundary layers. *Phys. Fluids* **18**, 289–297.

Bake, S., Ivanov, A. V., Fernholz, H. H., Neeman, K. & Kachanov, Y. 2002 Receptivity of boundary layers to three-dimensional disturbances. *Eur. J. Mech.* B *Fluids* **21**, 29–48.

Benney, D. J. 1961 A nonlinear theory for oscillations in a parallel flow. *J. Fluid Mech.* **10**, 208–236.

Berlin, S., Lundbladh, A. & Henningson, D. 1994 Spatial simulations of oblique transition in a boundary layer. *Phys. Fluids* **6**, 1949–1951.

Boiko, A. V., Westin, J. A., Klingmann, B. G. B., Kozlov, V. V. & Alfredsson, P. H. 1994 Experiments in a boundary layer subjected to free stream turbulence. Part 2. The role of TS-waves in the transition process. *J. Fluid Mech.* **281**, 219–245.

Elofsson, P. A. & Alfredsson, P. H. 1998 An experimental study of oblique transition in plane Poiseuille flow. *J. Fluid Mech.* **358**, 177–202.

Gaster, M. 1975 A theoretical model of a wave packet in the boundary layer on a flat plate. *Proc. R. Soc. Lond.* A **347**, 271–289.

Gaster, M. 1978 The physical process causing breakdown to turbulence. In *12th Naval Hydrodyn. Symp.* Washington.

Gaster, M. 1990 The nonlinear phase of wave growth leading to chaos and breakdown to turbulence in a boundary layer as an example of an open system. *Proc. R. Soc. Lond.* A **430**, 3–24.

Gaster, M. & Grant, I. 1975 An experimental investigation of the formation and development of a wavepacket in a laminar boundary layer. *Proc. R. Soc. Lond.* A **347**, 253–269.

https://doi.org/10.1017/S0022112004009188 Published online by Cambridge University Press

Henningson, D. S., Lundbladh, A. & Johansson, A. V. 1993 A mechanism for bypass transition from localized disturbances in wall-bounded shear flows. *J. Fluid Mech.* **250**, 169–207.

Herbert, T. 1988 Secondary instability of boundary layers. *Annu. Rev. Fluid Mech.* **20**, 487–526.

Kachanov, Y. S. 1994 Physical mechanisms of laminar boundary layer transition. *Annu. Rev. Fluid Mech.* **26**, 411–482.

Kachanov, Y. S., Kozlov, V. V., Levchenko, V. Y. & Ramazanov, M. 1985 Nonlinear development of a wave in a boundary layer. In *Laminar–Turbulent Transition* (ed. V. V. Kozlov), pp. 61–73. Springer.

Klebanoff, P. S. & Tidstrom, K. D. 1959 Evolution of amplified waves leading to transition in a boundary layer with zero pressure gradient. *TR NASA* D-195.

Klebanoff, P. S., Tidstrom, K. D. & Sargent, L. M. 1962 The three-dimensional nature of boundary layer instability. *J. Fluid Mech.* **12**, 1–34.

Mack, L. M. 1984 Boundary-layer linear stability theory. In *Special Course on Stability and Transition of Laminar Flow. AGARD Rep.* 709.

Mack, L. M. 1985 Instability wave patterns from harmonic point sources and line sources in laminar boundary layers. In *Laminar–Turbulent Transition* (ed. V. V. Kozlov), pp. 125–132. Springer.

Medeiros, M. A. F. 2001 Influence of streamwise modulation on the evolution of a three-dimensional wavetrains. In *31st AIAA Fluid Dyn. Conf. Anaheim, June 2001*, pp. 1–8.

Medeiros, M. A. F. & Gaster, M. 1999*a* The influence of phase on the nonlinear evolution of wavepackets in boundary layers. *J. Fluid Mech.* **397**, 259–283.

Medeiros, M. A. F. & Gaster, M. 1999*b* The production of sub-harmonic waves in the nonlinear evolution of wavepackets in boundary layers. *J. Fluid Mech.* **399**, 301–318.

Nelson, G. & Craik, A. D. D. 1977 Growth of streamwise vorticity in unstable boundary layers. *Phys. Fluids* **20**, 698–700.

Reddy, S. C., Schmid, P. J., Baggett, J. S. & Henningson, D. S. 1998 On stability of streamwise streaks and transition thresholds in plane channel flows. *J. Fluid Mech.* **365**, 269–303.

Schmid, P. & Henningson, D. S 1992 A new mechanism for rapid transition involving a pair of oblique waves. *Phys. Fluids* A **9**, 1986–1989.

Schubauer, G. B. & Skramstad, H. K. 1943 Laminar boundary layer oscillations and transition on a flat plate. *TR NACA* 909, April.

Seifert, A. 1990 On the interaction of small amplitude disturbances emanating from discrete points in a Blasius boundary layer. PhD thesis, Tel-Aviv University.

Seifert, A. & Wygnanski, I. 1991 On the interaction of wave trains emanating from point sources in a Blasius boundary layer. In *Proc. Conf. on Boundary Layer Transition and Control, Cambridge, April 1991*. pp. 7.1–7.13 The Royal Aeronautical Society.

Shaikh, F. N. 1997 Investigation of transition to turbulence using white noise excitation and local analysis techniques. *J. Fluid Mech.* **348**, 29–83.

Stemmer, C., Kloker, K. & Wagner, S. 1998 DNS of harmonic point source disturbances in an airfoil boundary layer flow. In *29th AIAA Fluid Dyn. Conf. Albuquerque, NM, June 1998*, pp. 1–11.

Stuart, J. T. 1960 On the nonlinear mechanisms of wave disturbances in stable and unstable parallel flows. *J. Fluid Mech.* **9**, 1–21.

Westin, J. A., Boiko, A. V., Klingmann, B. G. B., Kozlov, V. V. & Alfredsson, P. H. 1994 Experiments in a boundary layer subjected to free stream turbulence. Part 1. Boundary layer structure and receptivity. *J. Fluid Mech.* **281**, 193–218.

Wiegand, T., Bestek, H., Wagner, S. & Fasel, H. 1995 Experiments on a wave train emanating from a point source in a laminar boundary layer. In *26th AIAA Fluid Dyn. Conf. San Diego, CA, June 1995*.

https://doi.org/10.1017/S0022112004009188 Published online by Cambridge University Press